Context-Dependent Relationships between Locus Coeruleus Firing Patterns and Coordinated Neural Activity in the Anterior Cingulate Cortex

Siddhartha Joshi and Joshua I. Gold

Department of Neuroscience, University of Pennsylvania, Philadelphia, PA 19104

CONTACT:

Siddhartha Joshi: thesidjoshi@gmail.com

Keywords:

neuronal variability, norepinephrine, neuromodulation, pairwise correlation, Fano factor

Abstract

Ascending neuromodulatory projections from the locus coeruleus (LC) affect cortical neural networks via the release of norepinephrine (NE). However, the exact nature of these neuromodulatory effects on neural activity patterns *in vivo* is not well understood. Here we show that in awake monkeys, LC activation is associated with changes in coordinated activity patterns in the anterior cingulate cortex (ACC). These relationships, which are largely independent of changes in firing rates of individual ACC neurons, depend on the type of LC activation: ACC pairwise correlations tend to be reduced when tonic (baseline) LC activity increases but are enhanced when external events drive phasic LC responses. Both relationships covary with pupil changes that reflect LC activation and arousal. These results suggest that modulations of information processing that reflect changes in coordinated activity patterns in cortical networks can result partly from ongoing, context-dependent, arousal-related changes in activation of the LC-NE system.

Introduction

Changes in brain state are associated with different levels of arousal, attention, motivation, surprise, and other factors that can affect the activity patterns of large populations of cortical neurons (McAdams and Maunsell, 1999; Purcell et al., 2012; Chang et al., 2012; Falkner et al., 2013; Downer et al., 2015; Ecker et al., 2016; Thiele et al., 2016). These changes are thought to result, in part, from the widespread release of neuromodulators (Aoki et al, 1987; Devauges and Sara, 1990; Schulz et al., 1993; Dalley et al., 2001; Bouret and Sara, 2005; Aston-Jones and Cohen, 2005; McGaughy et al., 2008; Salamone et al., 2009; Pinto et al., 2013; Varazzani et al., 2015; Khani and Rainer, 2016; Minces et al., 2017). Different neuromodulatory systems have different anatomical and physiological properties (Kupfermann, 1979; Aoki et al., 1987; Xiang et al., 1998; Flores-Hernandez et al, 2000; Fernández-Pastor and Meana, 2002; Ding and Perkel, 2002; Salgado et al., 2011; Herrero et al., 2013; Sugihara et al., 2016; Doyle and Meeks, 2017) that are thought to support their different roles in neural information processing (Abbott and Dayan, 1999; Nirenberg et al., 2003; Averbeck et al., 2006; Silver, 2010; Beck et al., 2011; Moreno-Bote et al., 2014; Kanitscheider et al., 2015; Lin et al., 2015; Rodenkirch et al., 2019). One prominent example is the locus coeruleus (LC)-norepinephrine (NE) system, whose diffuse projections throughout the brain, close relationship to the sleep-wake cycle, and relationship to electroencephalography (EEG) and pupillometry have led to several theories of its role in arousal-related modulations of cortical activity and function (Aston-Jones and Cohen, 2005; Aston-Jones and Bloom, 1981; Nieuwenhuis et al., 2011; Gilzenrat et al., 2010; Einhäuser et al., 2010; Murphy et al., 2011, 2014; Joshi et al., 2016; Joshi and Gold, 2020). However, only a small number of studies have shown direct relationships between (artificial) LC activity and cortical activity *in vivo* (e.g., Devilbiss and Waterhouse, 2011), limiting our understanding of the exact nature of these relationships.

Our aim was to test if and how endogenous tonic and sensory-driven phasic firing patterns in the LC relate to changes in neural activity patterns in the anterior cingulate cortex (ACC) of the primate brain. We targeted the ACC because it has strong reciprocal connectivity, both structural and functional, with the LC (Lewis et al., 1979; Morrison et al., 1979; Porrino and Goldman-Rakic, 1982; Jones et al., 1984; Fernández-Pastor et al., 2005; Gompf et al., 2010; Chandler and Waterhouse, 2012; Chandler et al., 2013; Tervo et al., 2014; Köhler et al., 2016; de Gee et al., 2017; Koga et al., 2020). Moreover, ACC neural activity can encode computations that underlie adaptive, goal-directed behaviors, including those that are also associated with indirect measures of LC-linked arousal, such as changes in pupil size and the P300 component of the event-related potential (ERP; Shima and Tanji, 1998; Gehring and Willoughby, 2002; Holroyd and Coles, 2002; Critchley et al., 2005; Matsumoto et al., 2007; Hayden et al., 2011; Shenhav et al., 2013; Ebitz and Platt, 2015; Sarafyazd and Jazayeri, 2019). Thus, interactions between LC and ACC neural activity patterns are likely to have broad behavioral relevance.

We recorded neural activity simultaneously in LC and ACC (Figure 1) and measured the pupil size of alert monkeys under two behavioral conditions: 1) performing a fixation task, and 2) performing a fixation task with randomly presented sounds. Both of these conditions have been associated with variations in arousal that covary with pupil size and can affect cognition and behavior (Aston-Jones and Bloom, 1981; Nieuwenhuis et al., 2011; Einhäuser et al., 2010; Gilzenrat et al., 2010; Murphy et al., 2011, 2014; Varazzani et al., 2015; Joshi et al., 2016). Conditioned on the firing (or lack of firing) of LC neurons, we measured activity patterns of individual neurons and coordinated activity between pairs of neurons in ACC, both of which govern the information-processing capacities of neural networks (Britten et al., 1992; Parker and Newsome, 1998; Cohen and Kohn, 2011; Moreno-Bote et al., 2014; Lin et al., 2015; Kohn et al., 2016). We were particularly interested in the timescales over which these features of neural activity in LC and ACC are related, which can provide insights into putative underlying

mechanisms. For example, neuromodulatory effects of the LC-NE system on ACC might be expected to have a relatively long time-course compared with the time course of typical synaptic events that are mediated by faster, glutamatergic neurotransmission (Feldman et al., 1997; McCormick and Prince, 1988; Wang and McCormick, 1993; Schmidt et al., 2013; Timmons et al., 2004). Below we show that such relatively long timescale relationships are evident between LC and ACC neural activity patterns, in particular changes in coordinated activity between pairs of ACC neurons, but not single neuron firing rates, that tend to decrease or increase in relation to spontaneous or evoked LC spikes, respectively.

Results

We analyzed neural activity from simultaneously measured sites in the LC (*n*=84 single units, including 78 simultaneously recorded pairs from 35 sites in monkey Sp; 84/80/31 in monkey Ci) and ACC (372/4,336/35 in monkey Sp; 275/2,875/31 in monkey Ci) and from LC-only recordings (71/12/73 in monkey Ci and 36/8/34 in monkey Oz) while the three monkeys maintained fixation on a visual spot. Our analyses focused on if and how mean spiking activity and individual and pairwise neuronal variability measured in one brain region (ACC or LC) related to neuronal activity in the other brain region (LC or ACC, respectively). To understand the temporal dynamics of these potential relationships, we systematically tested for effects across a broad range of time windows, from short windows of 100 ms, which are often interpreted in terms of neural synchrony, to longer windows of up to 1 s, which are consistent with typical timescales of slow neuromodulatory influences (Feldman et al., 1997; McCormick and Prince, 1988; Wang and McCormick, 1993; Schmidt et al., 2013; Timmons et al., 2004; Doiron et al., 2016). Because LC and ACC are connected reciprocally, we tested for relationships in both directions. However, as detailed below we found reliable relationships only for certain ACC firing patterns conditioned on LC activity and not vice versa. We therefore include most LC-conditioned ACC analyses in main figures and most ACC-conditioned LC analyses in supplemental figures.

Single-neuron activity during passive fixation

During passive fixation, LC neurons were weakly active, with no spikes measured on more than a third of all trials and otherwise a median [interquartile range, or IQR] firing rate of 1.8 [0.9–3.6] sp/s measured during 1.1 s of stable fixation (Figure 2A). For each session, we divided trials into six groups based on the given LC neuron's firing rate: trials with firing rate=0 (LC_{zero}), 1, 2, 3, and >=4 sp/s formed 5 groups, and all trials with firing rate >0 formed a sixth group ($LC_{non\text{-}zero}$). We then assessed ACC neural activity measured at the same time, conditioned on the LC group.

The mean and variance of ACC spike counts, along with their Fano factor (the ratio of variance over mean), increased steadily as a function of the duration of the counting window. These trends showed an apparent, small relationship with simultaneously measured LC spiking activity, such that the mean, variance, and Fano factor measured in the ACC was, on average, slightly higher for LC_{zero} versus $LC_{non\text{-}zero}$ trials. These relationships were statistically reliable in some cases when considering data from both monkeys combined together but not when considering data separately for each monkey (sign test for H_0: median difference between LC=0 and the given LC>0 condition computed per ACC unit, or ANOVA testing for an effect of LC firing rate group, p>0.05 in all cases; Figure 2B–G). Across ACC units, the reduction in Fano factor for LC_{zero} versus $LC_{non\text{-}zero}$ trials was associated strongly with a decrease in spike-count variance (Spearman's rho=0.85, p<0.05) and more weakly with a decrease in spike count (Spearman's rho=0.27, p<0.05; Figure 2 – Supplemental Figure 1).

In comparison, the mean, variance, and Fano factor of LC spike counts also increased steadily as a function of the duration of the counting window. However, none of these trends showed a statistically significant relationship to simultaneously measured ACC spiking activity (sign test and ANOVA, p>0.05 in all cases; Figure 2 – Supplemental Figure 2).

Coordinated activity during passive fixation

During passive fixation, pairs of neurons in ACC had coordinated spiking activity that varied considerably in sign and magnitude across pairs but also, as has been reported previously, depended systematically on the size of the time window used to count spikes (de la Rocha et al., 2007). Specifically, pairwise spike-count correlations (r_{sc}) in ACC had median [IQR] values of 0.02 [-0.01–0.04] using 100-ms counting windows and systematically increased and became more variable across pairs with larger counting windows up to 1 s (0.04 [-0.04–0.13]).

These ACC spike-count correlations also depended on the spiking activity of LC neurons measured at the same time. Specifically, the correlations were largest when:1) they were measured using relatively large time windows; 2) for ACC pairs that exhibited relatively large, positive correlations independent of LC firing; and 3) when the simultaneously recorded LC neuron was not active (Figures 3 and 4). For the example ACC pair illustrated in Figure 3A–C, r_{sc} was near zero when computed using relatively small time windows and then increased steadily with increasing bin sizes. The magnitude of these increases in r_{sc} with bin size was larger on trials in which the simultaneously measured LC neuron was not spiking versus spiking (Figure 3C).

The population of ACC pairs exhibited similar trends, with r_{sc} values tending to be smaller on $LC_{non\text{-}zero}$ versus LC_{zero} trials, particularly for larger time windows and for ACC pairs with non-negative LC-independent r_{sc} values. To visualize these effects, we first divided ACC pairs into terciles, according to their LC-independent r_{sc} values (Figure 4). Under these conditions, ACC r_{sc} values from the upper two terciles of LC-independent r_{sc} values were reduced by up to ~50% when computed on trials with at least one or more LC spike versus trials with no LC spikes (Figure 4D–F). There was no reliable, systematic difference in the magnitude of these effects with respect to the magnitude of $LC_{non\text{-}zero}$ activity (ANOVA, no group effect for LC firing rates >0, p>0.05 in all cases). These effects were not evident on shuffled trials, supporting the idea that the trial-by-trial relationships that we identified were not spurious reflections of the spiking statistics of each region considered separately (Figure 4–Figure Supplement 1). Furthermore, these LC-linked differences in ACC r_{sc} values did not result simply from changes in ACC neuron firing rates, because the two measures were unrelated (Figure 4–Figure Supplement 2).

To ensure that these results were not overly reliant on the terciles we used for the LC-independent r_{sc} values, we conducted complementary analyses that quantified the slope of the linear relationship between LC-dependent and LC-independent ACC r_{sc} values, computed separately for each time window and LC spike group as in Figure 4. These linear relationships measured for a range of time bins and comparing LC_{zero} versus $LC_{non\text{-}zero}$ conditions are shown in Figure 5. Consistent with the results shown in Figure 4, these slopes were consistently negative for both monkeys, implying larger reductions in ACC r_{sc} values related to LC spiking versus no-spiking conditions for larger LC-independent r_{sc} values (for each monkey tested separately: Spearman's *rho* < 0 and p<<0.05 for all bin sizes).

In contrast, spike-count correlations (r_{sc}) from simultaneously measured pairs of LC neurons did not depend systematically on concurrently measured ACC activity. In general, ACC-independent LC r_{sc} values were roughly similar to LC-independent ACC r_{sc} values, increasing steadily and becoming more variable as a function of the counting-window size; e.g., median [IQR] values were 0.01 [0.00–0.04] for 100-ms windows and 0.07 [0.00–0.2] for 1-s windows.

However, these values did not show reliable differences when compared on trials with high versus low ACC firing, analyzed in the same way as the LC-linked ACC r_{sc} values (Figure 4 – Figure Supplement 3). Thus, differences in single-unit LC activity were associated with differences in coordinated activity patterns of pairs of neurons in ACC, but differences in single-unit ACC activity were not associated with differences in coordinated activity patterns of pairs of neurons in LC.

Relationship between pupil diameter, LC spiking, and ACC coordinated activity during passive fixation

To further examine relationships between coordinated activity in ACC and activation of LC-linked arousal systems, we examined both relative to changes in pupil diameter. Consistent with our previous findings (Joshi et al., 2016), the timing of LC spiking was related to the phase of ongoing fluctuations in pupil diameter during passive fixation, such that LC spiking tended to be higher preceding dilation versus constriction. These modulations showed a systematic precession with dilation phase that corresponded to a delay of ~270 ms from the maximum modulation of LC activity to the relevant pupil change (Figure 6A; median of intercepts from linear regression of per-time-bin peaks of individual LC PETH's; bootstrapped 95% confidence interval from regression for each LC neuron = [177–353 ms]; for examples of pupil cycles, see Figure 6 – Figure Supplement 1).

Combined with our current findings that pairwise correlations in ACC tended to be smaller when LC is active during passive fixation, these results predicted that pairwise correlations in ACC should also vary systematically with the phase of ongoing fluctuations in pupil diameter. We found such a relationship between pupil phase and ACC r_{sc} values. Specifically, over a wide range of pupil phase, decreases in ACC r_{sc} followed increases in LC spiking (the fitted line in B is shifted to the right relative to the fitted line in A). These modulations also showed a systematic progression with pupil phase over roughly the same time frame as LC firing, implying that modulations of both LC firing and ACC r_{sc} had relatively fixed temporal relationships to pupil fluctuations and therefore to each other, as well (Figure 6B; Wilcoxon rank-sum test for H_0: equal LC PETH and ACC r_{sc} slopes, p=0.23).

Single-neuron activity in response to startling events

We further examined relationships between LC and ACC neural activity in the context of external events that can cause a startle response. We showed previously that a brief, loud sound played on randomly selected fixation trials ("beep trials") can elicit phasic pupil dilation as well as phasic responses from individual LC neurons (Joshi et al., 2016; evoked responses from an example LC neuron is shown in Figure 7A, and the LC population average from 3 monkeys is shown in Figure 7B). The beep stimulus also elicited a consistent, albeit weaker, response in the ACC (evoked responses from an example ACC neuron are shown in Figure 7D, and the ACC population average from 2 monkeys is shown in Figure 7E). The averaged ACC response included a slight excitation and then inhibition relative to baseline within 200 ms of stimulus presentation. Although we found some individual cases with a biphasic response (e.g., Figure 7D), the average phasic response likely resulted from the range of heterogeneous responses of individual ACC neurons (Figure 7 – Figure Supplement 1).

The startle events also caused transient reductions in the trial-to-trial variability (measured as the Fano factor) of spiking activity of individual neurons in both LC and ACC, with a slightly more sustained effect in the ACC (Figure 7C,F). This reduction in neuronal variability following the onset of a stimulus, also referred to as quenching, has been reported previously for neurons in a range of other cortical regions and for a range of task conditions (Churchland et al., 2010).

Coordinated activity in response to startling events

In the ACC, we found no evidence that the startling sound caused systematic changes in coordinated activity when measured independently of the LC response. Specifically, spike-count correlations were highly variable across ACC neuron pairs, with no statistically reliable, systematic differences when compared before versus after the beep (Comparing ACC r_{sc} before versus after beep for spikes measured in 1 s bins; Mann-Whitney U-test, p>0.05 for both monkeys).

In contrast, we found systematic relationships between the beep-induced changes in coordinated activity in the ACC and the strength of the simultaneously measured LC response. Specifically, LC neurons did not show a characteristic phasic response on every presentation of a startle stimulus: the median fraction of trials with a response that included a phasic increase and then decrease in spiking activity was 54% for Monkey Sp and 43% for monkey Ci (Figure 8 – Figure Supplement 1). Therefore, we tested if and how arousal-linked changes in ACC correlated activity depended on whether or not the simultaneously recorded LC neuron responded phasically to the startling sound. Specifically, we computed ACC r_{sc} in time bins of different sizes, separately for 1s preceding and 1s following the sound. For bin sizes <300 ms, ACC r_{sc} did not depend reliably on whether the sound drove an LC phasic response or not (Figure 8A, B). In contrast, for larger bin sizes, ACC r_{sc} tended to be larger after versus before the beep stimulus, but only for the subset of trials in which it also elicited the characteristic phasic LC response, for both monkeys (Figure 8A,B; sign-rank test for H_0: median pairwise difference between r_{sc} computed per pair after versus before the beep=0, p<0.05).

These modulations of ACC pairwise correlations did not reflect LC-driven differences in the stimulus-driven quenching of response variability in ACC, which was similar on trials with and without LC phasic responses (Fig. 8C,D; sign-rank test for H_0: median difference in Fano factor both before and after the beep=0, p>0.05 in all cases). These modulations also did not reflect simply transient differences in LC firing rates but rather specific differences between the presence and absence of the stimulus-evoked LC response. Specifically, we sorted non-beep trials according to average LC firing patterns that matched our criteria for identifying phasic and no-phasic beep responses. For these “fake-beep” trials, ACC r_{sc} did not depend on phasic elevations in LC firing (Figure 8E,F). The Fano factors calculated on these trials also did not show measureable differences for each condition (Figure 8G,H).

Relationship between pupil diameter, LC spiking, and ACC coordinated activity in response to startling events

We showed previously that the magnitude of beep-evoked LC phasic responses is correlated positively with the size of the evoked change in pupil diameter (Joshi et al., 2016). We reproduced those results in our current data set (Figure 9 – Figure Supplement 1). Consistent with this relationship, we also found that the difference in ACC r_{sc} after versus before the beep was larger on trials with a relatively large versus a relatively small (median split) evoked pupil response, for the longest spike-counting time bins (Wilcoxon sign-rank text for H_0: median difference across all pairs=0, p<0.05 for bin size=1000 ms). However, this relationship was secondary to the primary relationship between ACC r_{sc} and LC phasic activation: an ANOVA that accounted for the beep-induced change in ACC r_{sc} in terms of phasic versus no-phasic LC response, large versus small evoked pupil, and their interaction, identified only a main effect of phasic versus no-phasic LC response (p<0.05 for bin sizes = 600 and 700 ms). Thus, evoked changes in ACC r_{sc} reflected evoked changes in pupil size only insofar as those changes in pupil reflected LC activation.

DISCUSSION

We measured relationships between pupil-linked activation of the LC-NE system and changes in cortical neural activity patterns. Previously, we showed that changes in pupil size during passive, near fixation and when driven by external startling events covary with the timing of spiking activity in LC and parts of brainstem and cortex, including the ACC (Joshi et al., 2016). Other studies have shown that pupil size and other indirect measures of LC activation can also correspond to changes in correlated firing in sensory cortex under certain conditions (Reimer et al., 2014, 2016; Vinck et al., 2015; McGinley et al., 2015). We extended those findings, including one study that elicited changes in coordinated activity in cortex via manipulation of LC activity (Devilbiss and Waterhouse, 2011), by showing that LC neuronal activity is reliably associated with changes in correlated spiking activity (spike-count correlations, or r_{sc}) between pairs of neurons in ACC. We further showed that these LC-linked changes in ACC r_{sc} depend on the nature of the LC activation. During passive fixation and in the absence of controlled external inputs, tonic LC firing was associated with a reduction in ACC r_{sc}. In contrast, startling sounds drove brief, phasic increases in LC firing that were associated with an increase in ACC r_{sc}. Under both conditions, LC and pupil-linked changes in ACC r_{sc} were most pronounced over relatively long time windows (>500 ms) that are consistent with neuromodulatory timescales and thus might involve the effects of LC-mediated NE release in the ACC (Feldman et al., 1997; McCormick and Prince, 1988; Wang and McCormick, 1993; Schmidt et al., 2013; Timmons et al., 2004).

The context dependence of these effects implies that spontaneous versus sensory-evoked activation of the LC-NE system can have different effects on coordinated patterns of activity in cortical networks. These effects seem likely to involve the different LC firing patterns under these conditions, which for sensory-evoked activity include not just a large, transient increase in spike rate but also a reduction in spike-count variability and heterogenous relationships to pupil-linked changes in arousal (Joshi et al, 2016). In principle, different temporal patterns of NE release could mediate a range of synaptic effects via distinct NE receptor subtypes with different affinities and different spatial distributions in different parts of the brain (Aoki et al., 1987; Nicholas et al., 1993; Arnsten et al., 1998; Arnsten, 2000; Berridge et al., 2012; Berridge and Spencer, 2016). These synaptic effects can influence both excitatory and inhibitory neurons as well as astrocytes, resulting in changes in network dynamics in thalamus, cortex, and elsewhere (Segal and Bloom, 1976; Dillier et al., 1978; Waterhouse et al., 1980; McCormick and Prince, 1988; Wang and McCormick, 1993; McLean and Waterhouse, 1994; Fernández-Pastor and Meana, 2002; Salgado et al., 2011, 2016; Paukert et al., 2014; Guan et al., 2015; Schiemann et al., 2015; Sherpa et al., 2016; Garcia-Junco-Clemente et al., 2019; Aston-Jones and Cohen, 2005; Ohshima et al., 2017; Rodenkirch et al 2019). Exactly how these diverse mechanisms support context-dependent changes in coordinated activity patterns merits further study, perhaps by selectively controlling the magnitude and timing of NE release in cortex while assessing changes in coordinated activity and using biophysically inspired models to test hypotheses about the underlying mechanisms (de la Rocha et al., 2007; Doiron et al., 2016).

In contrast to the relationships that we identified between LC activation and coordinated ACC activity patterns, we did not find similarly reliable relationships between the spiking activity of individual neurons measured simultaneously in each of the two brain regions. For example, we found a slight increase in mean firing rates and marked reduction in the trial-to-trial variability of firing rates of individual units in the ACC in response to external stimuli, as has been reported previously (Churchland et al., 2010). However, these changes in single-unit ACC responses were not related reliably to properties of the concurrently measured LC response that we could measure and thus may involve mechanisms other than the LC-NE system. These findings do not appear to be consistent with previous work showing improvements in signal-to-noise ratios

in cortex in response to LC-NE activation or during states of higher versus lower global arousal (Kolta et al., 1978; Mclean and Waterhouse, 1994; Lee et al., 2018; Lombardo et al., 2018). This difference could reflect differences in the specific neurons that we targeted in ACC, the different task conditions we tested relative to previous studies, or both, and also merits further study.

What might be the function of LC- and arousal-linked changes in ACC correlations? In general, pairwise correlations can be useful or detrimental depending on a number of factors, many of which remain unexplored, particularly outside of sensory cortex (Averbeck et al., 2006; Cohen and Kohn, 2011; Kohn et al., 2016). For example, an increase in correlations is considered a possible mechanism for connecting neural populations over a range of spatial and temporal scales (Gray et al., 1989; Singer, 1999; Riehle et al., 1997). Some computational schemes can benefit from increases in correlated variability (Abbott and Dayan, 1999; Singer and Gray, 1995; Gray 1999; Kohn et al., 2016). However, an increase in correlations can also negatively impact the information coding capacity of a large neural population, particularly over longer integration windows (Zohary et al., 1994; Bair et al., 2001; Averbeck et al., 2006; Renart et al., 2010; but also see Nirenberg and Latham, 2003, and Moreno-Bote et al., 2014, for alternative interpretations). Global states such as arousal and attention (traditionally linked with LC-NE and cholinergic systems, respectively) can modulate cortical correlations (Cohen and Maunsell, 2009; Mitchell et al., 2009; Herrero et al., 2013; Schmidt et al., 2013). Some work has also suggested that correlations induced by common inputs must be actively decorrelated by the action of local recurrent excitation and inhibition, to preserve information fidelity (Ecker et al, 2010; Renart et al., 2010).

Our results suggest that both increases and decreases in coordinated neural activity patterns in cortex may be under context-dependent, moment-by-moment control of the LC-NE system. Event-driven phasic activation of LC could help to synchronize populations of cortical neurons by shifting them to a more correlated state. Conversely, during tonic (event-independent) firing, the LC-NE system could enhance information processing and signal-to-noise ratios by reducing cortical correlations. Further work is needed to identify if and how NE-mediated changes in network dynamics subserve these functions, particularly in the context of goal-directed behaviors that involve multiple brain regions, including LC and ACC, as well as other neuromodulator systems (Hayden et al., 2011; Varazzani et al., 2015; Ebitz and Platt, 2015; Alamia et al., 2019).

MATERIALS AND METHODS

Three adult male rhesus monkeys (*Macaca mulatta*) were used for this study (monkeys Oz, Ci, and Sp). All training, surgery and experimental procedures were performed in accordance with the NIH's Guide for the Care of Use of Laboratory Animals and were approved by the University of Pennsylvania Institutional Animal Care and Use Committee. The behavioral task and pupillometry recording and analysis techniques were identical to those we used previously (Joshi et al. 2016). Briefly, fixation trials were of variable length (1–5 s, uniformly distributed). The monkey was rewarded with a drop of water or diluted Kool-Aid for maintaining fixation until the end of the trial. On a subset of randomly chosen trials (~25%), after 1–1.5 s of fixation a sound (1 kHz, 0.5 s) was played over a speaker in the experimental booth ("beep trials"). The monkey was required to maintain fixation through the presentation of the sound, until the fixation point was turned off.

Electrophysiology

Each monkey was implanted with a recording cylinder that provided access to LC+ (the locus coeruleus and adjacent, NE-containing subcoeruleus nucleus; Sharma et al., 2010; Paxinos et al., 2008; Kalwani et al., 2014), inferior colliculus (IC), and superior colliculus (SC). The detailed methodology for targeting and surgically implanting the recording cylinder and then targeting, identifying, and confirming recording sites in these three brain regions is described in detail elsewhere (Kalwani et al., 2014; Joshi et al., 2016). Briefly, the LC was targeted initially using custom (Kalwani et al., 2009) and/or commercial software (Brainsight). Tracks were then refined using electrophysiological recordings and microstimulation in brain regions dorsal to LC. Neurons in the intermediate layers of SC (SC_i) exhibited spatial tuning on a visually guided saccade task and could elicit saccades via electrical microstimulation (Robinson, 1972; Sparks and Nelson, 1987). IC units exhibited clear responses to auditory stimuli. Activity in the trigeminal mesencephalic tract (me5), located immediately dorsal to the LC, showed distinct activity related to orofacial movements such as sipping. LC+ units had relatively long action-potential waveforms, were sensitive to arousing external stimuli (e.g., door knocking), and decreased firing when the monkey was drowsy (e.g., eyelids drooped; Aston-Jones et al., 1994; Bouret and Sara, 2004; Bouret and Richmond, 2009). Non-optimal tracks also helped with mapping; e.g., a more medial track could miss me5 but lead to the trochlear decussation with characteristic ramp-and-hold activity related to downward saccades. Likewise, tracks that encountered IC but not SC_i were likely too lateral and often missed me5 and LC. Sites were verified using MRI and assessing the effects of systemic injection of clonidine on LC+ responses in monkeys Oz and Ci and by histology with electrolytic lesions and electrode-tract reconstruction in monkey Oz (Kalwani et al., 2014). Recording and microstimulation in these brainstem-targeting tracks were conducted using custom-made electrodes (made from quartz-coated platinum-tungsten stock wire from Thomas Recording) and a Multichannel Acquisition Processor (Plexon, Inc.).

ACC cylinders were placed at Horsley-Clarke coordinates 33 mm anterior-posterior (AP), 8 mm lateral (L), in the left hemisphere for monkey Sp and in the right hemisphere for monkey Ci. For ACC recordings, we targeted the dorsal bank of the anterior cingulate sulcus, ~4–6 mm below the cortical surface. ACC tracks were planned and refined using MRI and Brainsight software, as well as by listening for characteristic patterns of white and gray matter during recordings in an initial series of mapping experiments. Recordings were conducted using either custom-made single electrodes or multicontact linear electrode arrays (8- and 16-channel V-probe, Plexon).

For each brain region, we recorded and analyzed data from all stable, well-isolated units that we encountered. Neural recordings were filtered between 100 Hz and 8 kHz for spikes (Plexon MAP). Spikes were sorted offline (Plexon offline sorter). Electrical microstimulation in SC_i

consisted of biphasic (negative-positive) pulses, 0.3 ms long, 100 ms in duration, and delivered at 300 Hz via a Grass S-88 stimulator through a pair of constant-current stimulus isolation units (Grass SIU6) that were linked together to generate the biphasic pulse.

Data Analysis

For each recorded neuron, we considered spiking activity only during stable fixation, defined as a 1.1-s window that began 1 s after attaining fixation in which the monkey's gaze remained within a square window 0.2° per side centered on the fixation point. To assess ACC spiking activity patterns conditioned on LC activation, we divided trials within each session based on whether the single LC neuron from which recordings were being made either did ($LC_{non\text{-}zero}$) or did not (LC_{zero}) produce at least one action potential during stable fixation. We also divided session trials into four additional groups of trials in which the LC neuron fired 1, 2, 3 and >=4 spikes.

We used 10 bin sizes ranging from 100 ms to 1 s, spaced logarithmically, to count spikes. The mean spike count, variance of spike counts, and the Fano factor (the ratio of the variance to the mean of spike counts) for each neuron were calculated across trials for each bin size. Pairwise spike-count correlations (r_{sc}) were calculated for each bin size as follows. First, trial spike counts from each neuron in the pair were z-scored, and trials on which the response of either neuron was >3 standard deviations different from its mean were removed to avoid effects of outlier responses (Kohn and Smith, 2005; Smith and Kohn, 2008). Then, the MATLAB function corrcoef was used to obtain the Pearson correlation coefficient. Shuffled estimates were made by calculating r_{sc} from pairs of neurons with spike-count vectors generated from randomly selected trials for each neuron.

ACC r_{sc} values were calculated for all trials for each pair of well-isolated neurons, independently of spiking in LC and also separately for trials divided into groups depending on spiking in LC (LC_{zero} and the 5 LC>0 groups). The LC-independent r_{sc} values collected from all pairs and measured using ACC spikes counted using each time bin were divided into terciles that corresponded broadly to pairs that were negatively correlated (tercile 1), uncorrelated (tercile 2), or positively correlated (tercile 3). This analysis allowed us to assess whether changes in r_{sc} in one region associated with spiking in the other region depended on the pairs being correlated to begin with or not.

ACKNOWLEDGMENTS

We thank Long Ding, Adrian Radillo, Alice Dallstream, Kyra Schapiro, David Kleinfeld, and Takahiro Doi for valuable comments, Rishi Kalwani for piloting the LC/fixation studies, and Jean Zweigle for expert animal care and training. Funded by R21 MH107001.

Author Contributions

SJ collected the data; SJ and JIG designed the study, analyzed the data, and wrote the paper.

REFERENCES

Abbott, L.F., and Dayan, P. (1999). The effect of correlated variability on the accuracy of a population code. Neural Comput. 11, 91–101.

Alamia, A., VanRullen, R., Pasqualotto, E., Mouraux, A., and Zenon, A. (2019). Pupil-linked arousal responds to unconscious surprisal. J. Neurosci. (May 6 EPub ahead of print).

Aoki, C., Joh, T.H., and Pickel, V.M. (1987). Ultrastructural localization of beta-adrenergic receptor-like immunoreactivity in the cortex and neostriatum of rat brain. Brain Res. 437:264-282.

Arnsten, A.F., Steere, J.C., Jentsch, D.J., and Li, B.M. (1998). Noradrenergic influences on prefrontal cortical cognitive function: opposing actions at postjunctional alpha 1 versus alpha 2-adrenergic receptors. Adv Pharmacol. 42:764-767.Arnsten AF. (2000). Through the looking glass: differential noradenergic modulation of prefrontal cortical function. Neural Plast. 7:133-146.

Arnsten, A.F. (2000). Through the looking glass: differential noradenergic modulation of prefrontal cortical function. Neural Plast. 7:133-146.

Averbeck, B.B., Latham, P.E. and Pouget, A. (2006). Neural correlations, population coding and computation. Nat. Rev. Neurosci. 7, 358–366.

Aston-Jones, G., Bloom, F.E. (1981). Norepinephrine-containing locus coeruleus neurons in behaving rats exhibit pronounced responses to non-noxious environmental stimuli. J Neurosci. (8):887-900.

Aston-Jones, G., Rajkowski, J., Kubiak, P., and Alexinsky, T. (1994). Locus coeruleus neurons in monkey are selectively activated by attended cues in a vigilance task. J. Neurosci. 14, 4467–4480.

Aston-Jones, G., and Cohen, J.D. (2005). An integrative theory of locus coeruleus-norepinephrine function: adaptive gain and optimal performance. Annu Rev Neurosci. 28:403-450.

Bair, W., Zohary, E., and Newsome, W.T. (2001). Correlated firing in macaque visual area MT: time scales and relationship to behavior. J Neurosci. 21:1676-1697.

Beck, J,. Bejjanki, V.R., and Pouget, A. (2011). Insights from a simple expression for linear fisher information in a recurrently connected population of spiking neurons Neural Computation 23:1484–1502.

Berridge, C.W., Shumsky, J.S., Andrzejewski, M.E., McGaughy, J.A., Spencer, R.C., Devilbiss, D.M., and Waterhouse, B.D. (2012). Differential sensitivity to psychostimulants across prefrontal cognitive tasks: differential involvement of noradrenergic α_1 - and α_2-receptors. Biol Psychiatry. 71:467-473.

Berridge, C.W., and Spencer, R.C. (2016) Differential cognitive actions of norepinephrine a2 and a1 receptor signaling in the prefrontal cortex. Brain Res. 1641(Pt B):189-196.

Bouret, S., and Richmond, B.J. (2009). Relation of locus coeruleus neurons in monkeys to Pavlovian and operant behaviors. J. Neurophysiol. 101, 898–911.

Bouret, S., and Sara, S.J. (2004). Reward expectation, orientation of attention and locus coeruleus-medial frontal cortex interplay during learning. Eur. J. Neurosci. 20, 791–802.

Bouret, S., and Sara, S.J. (2005). Network reset: a simplified overarching theory of locus coeruleus noradrenaline function. Trends Neurosci. 28:574-582.

Britten, K.H., Shadlen, M.N., Newsome, W.T., Movshon, J.A. (1992). The analysis of visual motion: a comparison of neuronal and psychophysical performance. J Neurosci. 12:4745-4765.

Chandler, D., and Waterhouse, B.D. (2012). Evidence for broad versus segregated projections from cholinergic and noradrenergic nuclei to functionally and anatomically discrete subregions of prefrontal cortex. Front Behav Neurosci. 2012 May 21;6:20.

Chandler, D.J., Lamperski, C.S., and Waterhouse, B.D. (2013). Identification and distribution of projections from monoaminergic and cholinergic nuclei to functionally differentiated subregions of prefrontal cortex. Brain Res. 1522:38-58.

Chang, M.H., Armstrong, K.M., and Moore, T. (2012). Dissociation of response variability from firing rate effects in frontal eye field neurons during visual stimulation, working memory, and attention. J Neurosci. 32(6):2204-16.

Churchland, M.M., Yu, B.M., Cunningham, J.P., Sugrue, L.P., Cohen, M.R., Corrado, G.S., Newsome, W.T., Clark, A.M., Hosseini, P., Scott, B.B., Bradley, D.C., Smith, M.A., Kohn, A., Movshon, J.A., Armstrong, K.M., Moore, T., Chang, S.W., Snyder, L.H., Lisberger, S.G., Priebe, N.J., Finn, I.M., Ferster, D., Ryu, S.I., Santhanam, G., Sahani, M., and Shenoy, K.V. (2010). Stimulus onset quenches neural variability: a widespread cortical phenomenon. Nat Neurosci. 13:369-78.

Cohen, M.R., and Kohn, A. (2011). Measuring and interpreting neuronal correlations. Nat Neurosci. 14:811-819.

Cohen, M.R., and Maunsell, J.H. (2009). Attention improves performance primarily by reducing interneuronal correlations. Nat. Neurosci. 12:1594–1600.

Critchley, H.D., Tang, J., Glaser, D., Butterworth, B., and Dolan, R.J. (2005). Anterior cingulate activity during error and autonomic response. Neuroimage. 27:885-895.

Dalley, J.W., McGaughy, J., O'Connell, M.T., Cardinal, R.N., Levita, L., and Robbins, T.W. (2001). Distinct changes in cortical acetylcholine and noradrenaline efflux during contingent and noncontingent performance of a visual attentional task. J Neurosci. 21:4908-4914.

de Gee, J.W., Colizoli, O., Kloosterman, N.A., Knapen, T., Nieuwenhuis, S., and Donner, T.H. (2017). Dynamic modulation of decision biases by brainstem arousal systems. Elife. 6. pii: e23232.

de la Rocha, J., Doiron, B., Shea-Brown, E., Josić, K., and Reyes, A. (2007). Correlation between neural spike trains increases with firing rate. Nature. 448(7155):802-806.

Devauges, V., and Sara, S.J. (1990) Activation of the noradrenergic system facilitates an attentional shift in the rat. Behav Brain Res. 39:19-28.

Devilbiss DM1, Waterhouse BD. (2011). Phasic and tonic patterns of locus coeruleus output differentially modulate sensory network function in the awake rat. J Neurophysiol. 105:69-87.

Dillier, N., Laszlo, J., Müller, B., Koella, W.P., and Olpe, H.R. (1978). Activation of an inhibitory noradrenergic pathway projecting from the locus coeruleus to the cingulate cortex of the rat. Brain Res. 154, 61–68.

Ding, L., and Perkel, D.J. (2002). Dopamine modulates excitability of spiny neurons in the avian basal ganglia. J Neurosci. 22:5210-5218.

Doiron, B., Litwin-Kumar, A., Rosenbaum, R., Ocker, G.K., Josić, K. (2016). The mechanics of state-dependent neural correlations. Nat Neurosci. 19:383-393.

Downer, J.D., Niwa, M., and Sutter, M.L. (2015). Task engagement selectively modulates neural correlations in primary auditory cortex. J Neurosci. 35(19):7565-7574.

Doyle, W.I., and Meeks J.P. (2017). Heterogeneous effects of noradrenaline on spontaneous and stimulus-driven activity in the male accessory olfactory bulb. J Neurophysiol. 117:1342-1351.

Ebitz, R.B., and Platt, M.L. (2015). Neuronal activity in primate dorsal anterior cingulate cortex signals task conflict and predicts adjustments in pupil-linked arousal Neuron 85(3):628-640.

Ecker, A.S., Berens, P., Keliris, G.A., Bethge, M., Logothetis, N.K., and Tolias, A.S. (2010). Decorrelated neuronal firing in cortical microcircuits. Science. 327:584-587.

Ecker, A.S., Denfield, G.H., Bethge, M., and Tolias, A.S. (2016). On the Structure of Neuronal Population Activity under Fluctuations in Attentional State. J Neurosci. 36(5):1775-1789.

Einhäuser, W., Koch, C., and Carter, O.L. (2010). Pupil dilation betrays the timing of decisions. Front. Hum. Neurosci. 4, 18.

Falkner, A.L., Goldberg, M.E., and Krishna, B.S. (2013). Spatial representation and cognitive modulation of response variability in the lateral intraparietal area priority map. J Neurosci. 33(41):16117-16130.

Feldman, R.S., Meyer, J.S., Quenzer, L.F. In: Principles of Neuropsychopharmacology 1st Edition (Sinauer, 1997).

Fernández-Pastor, B., and Meana J.J. (2002). In vivo tonic modulation of the noradrenaline release in the rat cortex by locus coeruleus somatodendritic alpha(2)-adrenoceptors. Eur J Pharmacol. 442(3):225-229.

Fernández-Pastor, B., Mateo, Y., Gómez-Urquijo, S., and Javier Meana, J. (2005). Characterization of noradrenaline release in the locus coeruleus of freely moving awake rats by in vivo microdialysis. Psychopharmacology (Berl).180(3):570-579.

Flores-Hernandez, J., Hernandez, S., Snyder, G.L., Yan, Z., Fienberg, A.A., Moss, S.J., Greengard, P., and Surmeier, D.J. (2000). D(1) dopamine receptor activation reduces GABA(A) receptor currents in neostriatal neurons through a PKA/DARPP-32/PP1 signaling cascade. J Neurophysiol. 83:2996-3004.

Garcia-Junco-Clemente, P., Tring, E., Ringach, D.L., and Trachtenberg, J.T. (2019). State-Dependent Subnetworks of Parvalbumin-Expressing Interneurons in Neocortex. Cell Rep. 26:2282-2288

Gehring, W.J., and Willoughby, A.R. (2002). The medial frontal cortex and the rapid processing of monetary gains and losses. Science 295:2279–2282

Gilzenrat, M.S., Nieuwenhuis, S., Jepma, M., and Cohen, J.D. (2010). Pupil diameter tracks changes in control state predicted by the adaptive gain theory of locus coeruleus function. Cogn. Affect. Behav. Neurosci. 10, 252–269.

Gompf, H.S., Mathai, C., Fuller, P.M., Wood, D.A., Pedersen, N.P., Saper, C.B., and Lu, J. (2010). Locus ceruleus and anterior cingulate cortex sustain wakefulness in a novel environment. J Neurosci. 30:14543-14551.

Gray, C.M. (1999). The temporal correlation hypothesis of visual feature integration: still alive and well. Neuron 24:31-47, 111–125.

Gray, C.M., König, P., Engel, A.K., and Singer, W. (1989) Oscillatory responses in cat visual cortex exhibit inter-columnar synchronization which reflects global stimulus properties. Nature. 1989 Mar 23;338:334-337.

Guan, D., Armstrong, W.E., Foehring, R.C. (2015). Electrophysiological properties of genetically identified subtypes of layer 5 neocortical pyramidal neurons: Ca^{2+} dependence and differential modulation by norepinephrine. J Neurophysiol. 113:2014-2032

Hayden, B.Y., Heilbronner, S.R., Pearson, J.M., and Platt, M.L. (2011). Surprise signals in anterior cingulate cortex: neuronal encoding of unsigned reward prediction errors driving adjustment in behavior. J Neurosci. 31:4178-4187.

Herrero, J.L., Gieselmann, M.A., Sanayei, M., and Thiele, A. (2013). Attention-induced variance and noise correlation reduction in macaque V1 is mediated by NMDA receptors. Neuron. 78:729-739.

Holroyd, C.B., and Coles, M.G. (2002). The neural basis of human error processing: reinforcement learning, dopamine, and the error-related negativity. Psychol Rev 109:679–709.

Jones, R.S., and Olpe, H.R. (1984). Activation of the noradrenergic projection from locus coeruleus reduces the excitatory responses of anterior cingulate cortical neurones to substance P. Neuroscience. 13(3):819-825.

Joshi, S., Li, Y., Kalwani, R.M., and Gold, J.I. (2016). Relationships between Pupil Diameter and Neuronal Activity in the Locus Coeruleus, Colliculi, and Cingulate Cortex. Neuron. 89(1):221-234.

Joshi S., Gold J.I. (2020). Pupil Size as a Window on Neural Substrates of Cognition. Trends Cogn Sci. 24:466-480.Kalwani, R.M., Bloy, L., Elliott, M.A., and Gold, J.I. (2009). A method for localizing microelectrode trajectories in the macaque brain using MRI. J. Neurosci. Methods 176, 104–111.

Kalwani, R.M., Joshi, S., and Gold, J.I. (2014). Phasic activation of individual neurons in the locus ceruleus/subceruleus complex of monkeys reflects rewarded decisions to go but not stop. J. Neurosci. 34, 13656–13669.

Kanitscheider, I., Coen-Cagli, R., Kohn, A., and Pouget, A. (2015). Measuring Fisher information accurately in correlated neural populations. PLoS Comput Biol. 11:e1004218.

Khani, A., and Rainer, G. (2016). Neural and neurochemical basis of reinforcement-guided decision making. J Neurophysiol. 116:724-741.

Koga, K., Yamada, A., Song, Q., Li, X.H., Chen, Q.Y., Liu, R.H., Ge, J., Zhan, C, Furue, H., Zhuo, M., Chen, T. (2020). Ascending noradrenergic excitation from the locus coeruleus to the anterior cingulate cortex. Mol Brain. 13(1):49.

Köhler, S., Bär, K.J., and Wagner, G. (2016). Hum Brain Mapp. 37(6):2305-18. Differential involvement of brainstem noradrenergic and midbrain dopaminergic nuclei in cognitive control.

Kohn, A., and Smith M.A. (2005). Stimulus dependence of neuronal correlation in primary visual cortex of the macaque. J Neurosci. 25:3661-3673.

Kohn, A., Coen-Cagli, R., Kanitscheider, I., and Pouget, A. (2016). Correlations and Neuronal Population Information. Annu Rev Neurosci. 39:237-256

Kolta, A., Diop, L., and Reader, T.A. (1987). Noradrenergic effects on rat visual cortex: single-cell microiontophoretic studies of alpha-2 adrenergic receptors. Life Sci. 41:281-289.

Kupfermann, I. (1979). Modulatory actions of neurotransmitters. Annu Rev Neurosci 2:447-465.

Lee, V., Pawlisch, B.A., Macedo-Lima, M., Remage-Healey, L. (2018). Norepinephrine enhances song responsiveness and encoding in the auditory forebrain of male zebra finches. J Neurophysiol. 119:209-220.

Lewis, M.S., Molliver, M.E., Morrison, J.H., and Lidov, H.G. (1979). Complmentarity of dopaminergic and noradrenergic innervation in anterior cingulate cortex of the rat. Brain Res. 164:328-33.

Lin, I.C., Okun, M., Carandini, M., and Harris, K.D. (2015). The Nature of Shared Cortical Variability. Neuron. 87:644-656.

Lombardo, J.A., Macellaio, M.V., Liu, B., Palmer, S.E., and Osborne, L.C. (2018). State dependence of stimulus-induced variability tuning in macaque MT. PLoS Comput Biol. 14(10):e1006527.

McLean, J., and Waterhouse, B.D. (1994). Noradrenergic modulation of cat area 17 neuronal responses to moving visual stimuli. Brain Res. 1994 Dec 19;667(1):83-97.

Matsumoto, M., Matsumoto, K., Abe, H., and Tanaka, K. (2007). Medial prefrontal cell activity signaling prediction errors of action values. Nat Neurosci 10:647–656.

McAdams, C.J., and Maunsell, J.H.R. (1999). Effects of attention on orientation-tuning functions of single neurons in macaque cortical area V4. J Neurosci 19:431-441.

McCormick, D.A, and Prince, D.A. (1988). Noradrenergic modulation of firing pattern in guinea pig and cat thalamic neurons, in vitro. J Neurophysiol. 59:978-96.

McGaughy, J., Ross, R.S., and Eichenbaum, H. (2008). Noradrenergic, but not cholinergic, deafferentation of prefrontal cortex impairs attentional set-shifting. Neuroscience. 153:63-71.

McGinley, M.J., David, S.V., and McCormick, D.A. (2015). Cortical membrane potential signature of optimal states for sensory signal detection. Neuron 87, 179–192.

Minces, V., Pinto, L., Dan, Y., and Chiba, A.A. (2017). Cholinergic shaping of neural correlations. Proc Natl Acad Sci USA. 114:5725-5730.

Mitchell, J.F., Sundberg, K.A., and Reynolds, J.H. (2009). Spatial attention decorrelates intrinsic activity fluctuations in macaque area V4. Neuron 63:879–88

Moreno-Bote, R., Beck, J., Kanitscheider I., Pitkow, X., Latham, P., and Pouget, A. (2014). Information-limiting correlations. Nat Neurosci. 17(10):1410-7.

Morrison, J.H., Molliver, M.E., Grzanna, R., and Coyle, J.T. (1979). Noradrenergic innervation patterns in three regions of medial cortex: an immunofluorescence characterization. Brain Res Bull. 4:849-857.

Murphy, P.R., Robertson, I.H., Balsters, J.H., and O'Connell, R.G. (2011). Pupillometry and P3 index the locus coeruleus-noradrenergic arousal function in humans. Psychophysiology 48, 1532–1543.

Murphy, P.R., O'Connell, R.G., O'Sullivan, M., Robertson, I.H., and Balsters, J.H. (2014). Pupil diameter covaries with BOLD activity in human locus coeruleus. Hum. Brain Mapp. 35, 4140–4154.

Nicholas, A.P., Pieribone. V., and Hokfelt, T. (1993). Distributions of mRNAs for alpha-2 adrenergic receptor subtypes in rat brain: an in situ hybridization study. J Comp Neurol. 328:575–575

Nieuwenhuis, S., De Geus, E.J., and Aston-Jones, G. (2011). The anatomical and functional relationship between the P3 and autonomic components of the orienting response. Psychophysiology 48, 162–175.

Nirenberg, S. & Latham, P.E. (2003). Decoding neuronal spike trains: how important are correlations? Proc. Natl. Acad. Sci. USA 100, 7348–7353.

Ohshima, M., Itami, C., Kimura, F. (2017). The α2A -adrenoceptor suppresses excitatory synaptic transmission to both excitatory and inhibitory neurons in layer 4 barrel cortex. J Physiol. 595:6923-6937.

Parker, A.J. and Newsome, W.T. (1998). Sense and the single neuron: probing the physiology of perception. Ann. Rev. Neurosci. 1998;21:227-277.

Paukert, M., Agarwal, A., Cha, J., Doze, V.A., Kang, J.U., and Bergles, D.E. (2014). Norepinephrine controls astroglial responsiveness to local circuit activity. Neuron. 82:1263-70.

Paxinos, G., Huang, X.-F., Petrides, M., and Toga, A. (2008). The Rhesus Monkey Brain in Stereotaxic Coordinates, Second Edition (Academic Press).

Pinto, L., Goard, M.J., Estandian, D., Xu, M., Kwan, A.C., Lee, S.H., Harrison, T.C., Feng, G., and Dan, Y. (2013). Fast modulation of visual perception by basal forebrain cholinergic neurons. Nat Neurosci. 16:1857-1863.

Porrino, L.J., and Goldman-Rakic, P.S. (1982). Brainstem innervation of prefrontal and anterior cingulate cortex in the rhesus monkey revealed by retrograde transport of HRP. J Comp Neurol. 205(1):63-76.

Purcell, B.A., Heitz, R.P., Cohen, J.Y., and Schall, J.D. (2012). Response variability of frontal eye field neurons modulates with sensory input and saccade preparation but not visual search salience. J Neurophysiol. 108(10):2737-2750.

Reimer, J., Froudarakis, E., Cadwell, C.R., Yatsenko, D., Denfield, G.H., and Tolias, A.S. (2014). Pupil fluctuations track fast switching of cortical states during quiet wakefulness. Neuron. 84:355-362.

Reimer, J., McGinley, M.J., Liu, Y., Rodenkirch, C., Wang, Q., McCormick, D.A., and Tolias, A.S. (2016) Pupil fluctuations track rapid changes in adrenergic and cholinergic activity in cortex. Nat Commun. 7:13289.

Renart, A., de la Rocha, J., Bartho, P., Hollender, L., Parga, N., Reyes, A., and Harris, K.D. (2010) The asynchronous state in cortical circuits. 327:587-590.

Riehle, A., Grün, S., Diesmann, M., and Aertsen, A. (1997). Spike synchronization and rate modulation differentially involved in motor cortical function. Science. 278:1950-1953.

Robinson, D.A. (1972) Eye movements evoked by collicular stimulation in the alert monkey. Vision Res. 1972 Nov;12(11):1795-808.

Rodenkirch, C., Liu, Y., Schriver, B.J., and Wang, Q. (2019). Locus coeruleus activation enhances thalamic feature selectivity via norepinephrine regulation of intrathalamic circuit dynamics. Nat Neurosci. 22:120-133.

Sarafyazd, M., and Jazayeri, M. (2019). Hierarchical reasoning by neural circuits in the frontal cortex. Science. 364: eaav8911.

Salamone, J. D., Correa, M., Farrar, A. M., Nunes, E. J., and Pardo, M. (2009). Dopamine, behavioral economics, and effort. Front. Behav. Neurosci. 3:13.

Salgado, H., Treviño, M., and Atzori, M. (2016). Layer- and area-specific actions of norepinephrine on cortical synaptic transmission. Brain Res. 1641(Pt B):163-176.

Salgado, H., Garcia-Oscos, F., Patel, A., Martinolich, L., Nichols, J.A., Dinh, L., Roychowdhury, S., Tseng, K.Y., and Atzori, M. (2011). Layer-specific noradrenergic modulation of inhibition in cortical layer II/III. Cereb Cortex. 21:212-221.

Schiemann, J., Puggioni, P., Dacre, J., Pelko, M., Domanski, A., van Rossum, M.C., and Duguid, I. (2015). Cellular mechanisms underlying behavioral state-dependent bidirectional modulation of motor cortex output. Cell Rep. 11:1319-30.

Schmidt, S.L., Chew, E.Y., Bennett, D.V., Hammad, M.A., and Fröhlich, F. (2013). Differential effects of cholinergic and noradrenergic neuromodulation on spontaneous cortical network dynamics. Neuropharmacology. 72:259-273.

Schultz W., Apicella P., and Ljungberg T. (1993). Responses of monkey dopamine neurons to reward and conditioned stimuli during successive steps of learning a delayed response task. J Neurosci. 13:900-913.

Segal, M., and Bloom, F.E. (1976). The action of norepinephrine in the rat hippocampus. III. Hippocampal cellular responses to locus coeruleus stimulation in the awake rat. Brain Res. 107, 499–511.

Sharma, Y., Xu, T., Graf, W.M., Fobbs, A., Sherwood, C.C., Hof, P.R., Allman, J.M., and Manaye, K.F. (2010). Comparative anatomy of the locus coeruleus in humans and nonhuman primates. J. Comp. Neurol. 518, 963–971.

Shenhav, A., Botvinick, M. M., & Cohen, J.D. (2013). The expected value of control: An integrative theory of anterior cingulate cortex function. Neuron, 79, 217–240.

Sherpa, A.D., Xiao F., Joseph, N., Aoki, C., and Hrabetova, S. (2016). Activation of β-adrenergic receptors in rat visual cortex expands astrocytic processes and reduces extracellular space volume. Synapse. 70:307-16

Shima, K., and Tanji, J. (1998). Role for cingulate motor area cells in voluntary movement selection based on reward. Science. 282(5392):1335-8.

Silver, R.A. (2010). Neuronal arithmetic. Nature Reviews Neuroscience 11:474–489

Singer, W, and Gray, CM. (1995). Visual feature integration and the temporal correlation hypothesis. Annu Rev Neurosci. 1995;18:555-586.

Singer, W. (1999). Neuronal synchrony: a versatile code for the definition of relations? Neuron. 24:49-65, 111-125.

Smith, M.A., and Kohn, A. (2008) Spatial and temporal scales of neuronal correlation in primary visual cortex. J Neurosci. 28:12591-12603

Sparks, D.L., and Nelson, J.S. (1987). Sensory and motor maps in the mammalian superior colliculus. Trends Neurosci. 10, 312–317.

Sugihara, H., Chen, N., and Sur, M. (2016).Cell-specific modulation of plasticity and cortical state by cholinergic inputs to the visual cortex. J Physiol Paris. 110:37-43.

Tervo, D.G.R., Proskurin, M., Manakov, M., Kabra, M., Vollmer, A., Branson, K., and Karpova, A.Y. (2014). Behavioral variability through stochastic choice and its gating by anterior cingulate cortex. Cell. 159:21-32.

Thiele, A., Brandt, C., Dasilva, M., Gotthardt, S., Chicharro, D., Panzeri, S., and Distler, C. (2016). Attention Induced Gain Stabilization in Broad and Narrow-Spiking Cells in the Frontal Eye-Field of Macaque Monkeys. J Neurosci. 36:7601-7612.

Timmons, S.D., Geisert, E., Stewart, A.E., Lorenzon, N.M., and Foehring R.C. (2004). alpha2-Adrenergic receptor-mediated modulation of calcium current in neocortical pyramidal neurons. Brain Res. 1014:184-196.

Varazzani, C., San-Galli, A., Gilardeau, S., and Bouret, S. (2015). Noradrenaline and dopamine neurons in the reward/effort trade-off: a direct electrophysiological comparison in behaving monkeys. J Neurosci. 35:7866-7877.

Vinck, M., Batista-Brito, R., Knoblich, U., and Cardin, J.A. (2015). Arousal and locomotion make distinct contributions to cortical activity patterns and visual encoding. Neuron 86, 740–754.

Wang, Z., and McCormick, D.A. (1993). Control of firing mode of corticotectal and corticopontine layer V burst-generating neurons by norepinephrine, acetylcholine, and 1S,3R-ACPD. J Neurosci. 13:2199-2216.

Waterhouse, B.D., Moises, H.C., and Woodward, D.J. (1980). Noradrenergic modulation of somatosensory cortical neuronal responses to iontophoretically applied putative neurotransmitters. Exp. Neurol. 69, 30-49.

Xiang, Z., Huguenard, J.R., and Prince D.A. (1998). Cholinergic switching within neocortical inhibitory networks. Science. 281:985-988.

Zohary, E., Shadlen, M.N., and Newsome, W.T. (1994). Correlated neuronal discharge rate and its implications for psychophysical performance. 370:140-143.

FIGURE LEGENDS

Figure 1. Recording site locations. (A) Approximately sagittal MRI section showing targeted recording locations in the ACC (areas 32, 24b, and 24c) and LC for monkey Ci (right), with the SC and IC shown for reference. For recording locations in monkeys Oz, Sp, and Ci (left hemisphere), see (Kalwani et al., 2014; Joshi et al., 2016). (B) Schematic of a coronal section showing structures typically encountered along electrode tracts to LC (adapted from Paxinos et al., 2008; Plate 90, Interaural 0.3; bregma 21.60).

Figure 2. ACC single-unit spike count statistics conditioned on simultaneously measured LC spiking. (A) LC single-unit firing-rate distribution measured in 1.1 s windows starting 1 s after the onset of stable fixation from all trials and recording sessions. The magenta and black bars indicate the proportion of trials with zero and >0 LC spikes, respectively. The diamond and horizontal bar indicate median and IQR, respectively, from trials with ≥1 spike. (B,C,D) ACC single-unit spike count (B), variance of the spike count (C), and Fano factor (variance/mean; D) from trials in which the simultaneously measured LC unit spiked as indicated in the legend in B. ACC spikes were counted in 10 equally spaced bins ranging from 100 ms to 1 s. Symbols and error bars are mean and sem of the values computed by pooling the data across all units recorded from both monkeys. (E,F,G) Percentage difference between each value from panels A,B,C, respectively, measured in each LC>0 condition (grayscale as in the legend in panel B) versus the LC=0 condition, relative to the value from the LC=0 condition. Bars and error bars are the median and bootstrapped 95% confidence interval of the distribution of values computed per ACC unit. Symbols above indicate $p<0.05$ for sign tests for: 1) H_0: median percent difference between LC_{zero} and $LC_{non\text{-}zero}$ conditions tested separately for each monkey=0 (+; none found), and 2) H_0: median difference between LC_{zero} and each LC spiking condition tested using data combined from both monkeys=0 (*).

Figure 3. Spike-count correlations (r_{sc}) of an example ACC pair conditioned on the spiking activity of a simultaneously recorded LC unit. (A) ACC spikes counted in a 100 ms-wide bin. (B) ACC spikes counted in a 1000 ms-wide bin. In A and B, square/diamond markers indicate data from trials in which the simultaneously recorded LC unit had zero/non-zero firing rates. Thin/thick lines are linear fits to these data points, respectively. (C) Spike-count correlation (r_{sc}) for the example ACC pair shown in A and B as a function of bin size, computed separately for trials in which the simultaneously recorded LC unit had zero/non-zero firing rates, as indicated in A.

Figure 4. Spike-count correlations (r_{sc}) within ACC conditioned on simultaneously measured LC spiking. (A,B,C) ACC r_{sc} plotted as a function of bin size for each LC spike condition indicated in the legend in A. The three panels separate data by ACC pairs with r_{sc} values that, without reference to LC firing and for each bin size, were in the lower (A), middle (B), or upper (C) tercile from all recorded ACC pairs. Symbols and error bars are mean and sem across the given set of ACC pairs. (D,E,F) Percentage difference in ACC r_{sc} between each LC>0 condition and the LC=0 condition, relative to the LC=0 condition, computed for each ACC pair and plotted separately for the terciles in A,B,C, respectively. Bars and error bars are median and bootstrapped 95% confidence intervals across the given set of ACC pairs. Symbols above indicate $p<0.05$ for sign tests for: 1) H_0: median difference between LC_{zero} and $LC_{non\text{-}zero}$

conditions tested separately for each monkey=0 (+), and 2) H_0: median difference between LC_{zero} and each LC spiking condition tested using data combined from both monkeys=0 (*).

Figure 5. Relationship between the difference in ACC r_{sc} for $LC_{non\text{-}zero}$ versus LC_{zero} conditions as a function of unconditioned ACC r_{sc}. Points are data from individual ACC pairs using spikes counted in different-sized time bins, as indicated. A 500-sample running mean is shown in red, and a linear fit to the data is shown in black. Slopes and *p*-values for H_0: slope=0 are shown above each panel ($p<0.05$ for all slopes tested separately for each monkey).

Figure 6. Spiking responses of LC neurons and correlated activity in ACC relative to pupil phase. (A) Mean LC spike rate (colormap, in sp/s z-scored per unit) computed in 500 ms-wide bins aligned to the time of occurrence of each pupil phase. For each complete pupil cycle, phase is defined with respect to the maximum rate of dilation (0°), the maximum size (90°), the maximum rate of constriction (180°), and the minimum size (270°; see Figure 6, Figure Supplement 1). Thus, the color shown at time=*t* (abscissa), phase=*p* (ordinate) corresponds to the mean spiking rate from all LC neurons that occurred in a 500 ms-wide bin centered *t* ms relative to the time of pupil phase *p*. Diagonal structure with a slope of ~-0.6 deg/ms implies a consistent relationship between LC firing and pupil phase for the given range of temporal offsets and pupil fluctuations, or hippus, that have a period of ~600 ms (Joshi et al 2016). (B) ACC r_{sc} aligned to pupil phase, computed as in A. In both panels, data are combined from all sessions for visualization. Lines are plotted using the median regression coefficients from statistically reliable linear fits (H_0: slope=0, $p<0.05$) to the maxima of phase-aligned LC spiking computed per unit (A; median [IQR] slope=-0.33 [-0.41 -0.30] deg/ms) and minima of the phase-aligned ACC r_{sc} computed per ACC pair (B; slope=-0.41 [-0.46 -0.35] deg/ms).

Figure 7. Neuronal responses to startling events (beep trials) in LC (left) and ACC (right). (A) Example LC unit spike raster and PSTH relative to beep onset. (B) LC population average response. (C) Fano factor as a function of time relative to beep onset, calculated in 200 ms windows. (D, E, F) ACC responses relative to beep onset plotted as in A–C. Lines and ribbons in B, C, E, and F indicate mean±sem across all trials for all monkeys.

Figure 8. Changes in correlated activity in ACC in response to startling events, conditioned on LC spiking. (A) ACC r_{sc} from before (gray markers) and after the beep (black markers) for trials in which LC had a phasic response, plotted as a function of the bin size used to count spikes in ACC. Circles and vertical lines show mean±sem across sessions and monkeys. (B) Data from trials in which LC did not respond to the beep, plotted as in A. (C, D) Fano factor before (gray) and after (black) the beep for ACC single neurons, plotted as in A and B. (E–G) Data from “fake-beep trials” (trials with no beep but sorted according to whether or not there was a transient increase in LC spiking comparable in magnitude to the beep-evoked response), plotted as in A–D. In all panels, + indicates sign-rank test for H_0: median difference in r_{sc} before versus after the beep for the given time bin, $p<0.05$ for each monkey tested separately.

Figure 9. Startle-linked changes in ACC correlations relative to LC and pupil responses. (A) ACC r_{sc} plotted as a function of bin size for trials in which a phasic LC response was accompanied by a large pupil dilation. (B) ACC r_{sc} for trials in which there was a large evoked

pupil dilation but no phasic LC response. (C) ACC r_{sc} for trials in which a phasic LC response was accompanied by a relatively smaller evoked pupil dilation. (D) ACC r_{sc} for trials in which there was a small evoked pupil dilation and no phasic LC response. All symbols and error bars are mean±sem across ACC pairs from both monkeys. * symbols at the top of each panel indicate sign-rank test for H_0: median difference in r_{sc} before versus after the beep for the given time bin, $p<0.05$ for each monkey tested separately. Red symbols at the top of A indicate bin-specific effects (ANOVA, $p<0.05$) of pupil size (large versus small; none significant), LC phasic response (yes versus no; +), and their interaction (none significant).

SUPPLEMENTAL FIGURES

Figure 2 – Figure Supplement 1. ACC single neuron spike count and variability conditioned on LC spiking (measured as differences between measurements from $LC_{non-zero}$ versus LC_{zero} trials). (A). Relationship between difference in Fano factor and difference in spike count. (B) Relationship between difference in Fano factor and difference in variance of spike count.

Figure 2 – Figure Supplement 2. LC single-unit spike count statistics conditioned on simultaneously measured ACC spiking. (A) ACC single-unit firing-rate distribution measured in 1.1 s windows starting 1 s after the onset of stable fixation from all trials and recording sessions. The circle and diamond symbols and lines indicate the median and IQR of trials defined as “low” and “high” ACC spike counts (median split per session), respectively. (B–D) LC single-unit (B) spike count, (C) variance of spike count, and (D) Fano factor (variance/mean) from trials in which the simultaneously measured ACC unit had low or high spiking activity as indicated by the markers defined in B. LC spikes were counted in 10 equally spaced bins ranging from 100 ms to 1 s. Symbols and error bars are mean ± sem of the values computed by pooling the data across all units recorded from both monkeys. (E,F,G) Percentage difference between each value from panels B,C,D, respectively, measured in the ACC low- versus high-spiking condition, relative to the low-spiking condition. In all cases, signtest for H_0: median percent change=0, $p>0.05$ for both monkeys tested separately or together.

Figure 4 – Figure Supplement 1. Confidence estimates of ACC r_{sc} conditioned on simultaneously measured LC spiking using shuffled trials. Solid markers show unshuffled ACC r_{sc} data conditioned on LC spiking, separated into terciles (panels) of LC-independent values, plotted as in Figure 4A–C for LC_{zero} and $LC_{non-zero}$ trials. Open markers show ACC r_{sc} from shuffled data. Bootstrapped 95% confidence intervals are plotted as vertical bars (too small for visibility in most cases).

Figure 4 – Figure Supplement 2. Relationship between LC-linked differences in ACC r_{sc} and ACC mean firing rate. For each simultaneously recorded pair of ACC units and single LC unit, the difference in ACC r_{sc} computed from $LC_{non-zero}$ versus LC_{zero} trials (ordinate) is plotted versus the difference in the mean spike rate of the two ACC units computed from $LC_{non-zero}$ versus LC_{zero} trials (abscissa). Spearman’s *rho*=0.007, $p=0.8$.

Figure 4 – Figure Supplement 3. Spike-count correlations (r_{sc}) within LC conditioned on simultaneously measured ACC spiking. (A,B,C) LC r_{sc} plotted as a function of bin size separately for trials in which the simultaneously recorded ACC unit had a relatively low or high firing rate, as indicated in A. The three panels separate data by LC pairs with r_{sc} values that, without reference to ACC firing and for each bin size, were in the lower (A), middle (B), or upper (C) tercile from all recorded LC pairs. Symbols and error bars are mean and sem across the given set of LC pairs. (D,E,F) Percentage difference in LC r_{sc} between ACC low versus ACC high conditions, relative to the ACC low condition, computed for each LC pair and plotted separately for the terciles in A,B,C, respectively. Bars and error bars are median and bootstrapped 95% confidence intervals across the given set of LC pairs. In all cases, sign test for H_0: median percent change=0, p>0.05 for both monkeys tested separately or together.

Figure 6 – Figure Supplement 1. Pupil phase examples. Example pupil traces from individual trials (rows) showing principal phases (left; 0°, 90°, 180°, and 270°) and intermediate sampled points (right) used in pupil analyses.

Figure 7 – Figure Supplement 1. ACC single-unit responses to the startle stimulus (beep). Average PSTHs aligned to beep onset from all units recorded from Monkey Sp (A) and monkey Ci (B).

Figure 8 – Figure Supplement 1. Consistency of LC responses to startling sounds. Histograms showing the proportion of LC neurons from monkey Sp (A) and Ci (B) that exhibited a characteristic phasic response followed by post-phasic suppression for the given proportion of beep trials. Arrows indicate median values.

Figure 9 – Figure Supplement 1. Relationship between startling sound-driven changes in pupil diameter and LC phasic activation. Distribution of correlation coefficients describing unit-specific relationships between the size of the pupil response and the size of the LC phasic response to beep presentation for monkey Sp (A) and Ci (B). Arrows indicate median values (sign-rank test for H_0: median=0, p<0.001 in both cases).

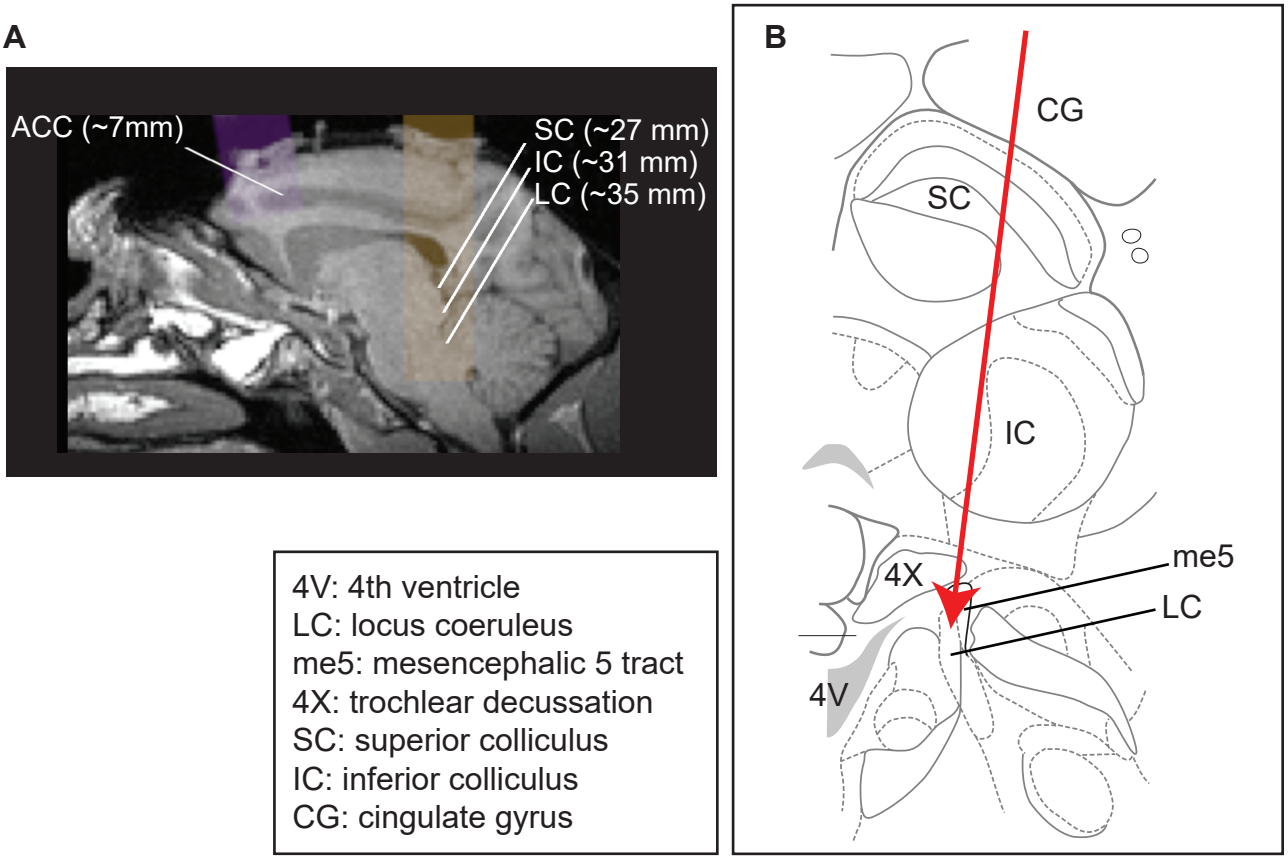

Figure 1. Recording site locations. (A) Approximately sagittal MRI section showing targeted recording locations in the ACC (areas 32, 24b, and 24c) and LC for monkey Ci (right), with the SC and IC shown for reference. For recording locations in monkeys Oz, Sp, and Ci (left hemisphere), see (Kalwani et al., 2014; Joshi et al., 2016). (B) Schematic of a coronal section showing structures typically encountered along electrode tracts to LC (adapted from Paxinos et al., 2008; Plate 90, Interaural 0.3; bregma 21.60).

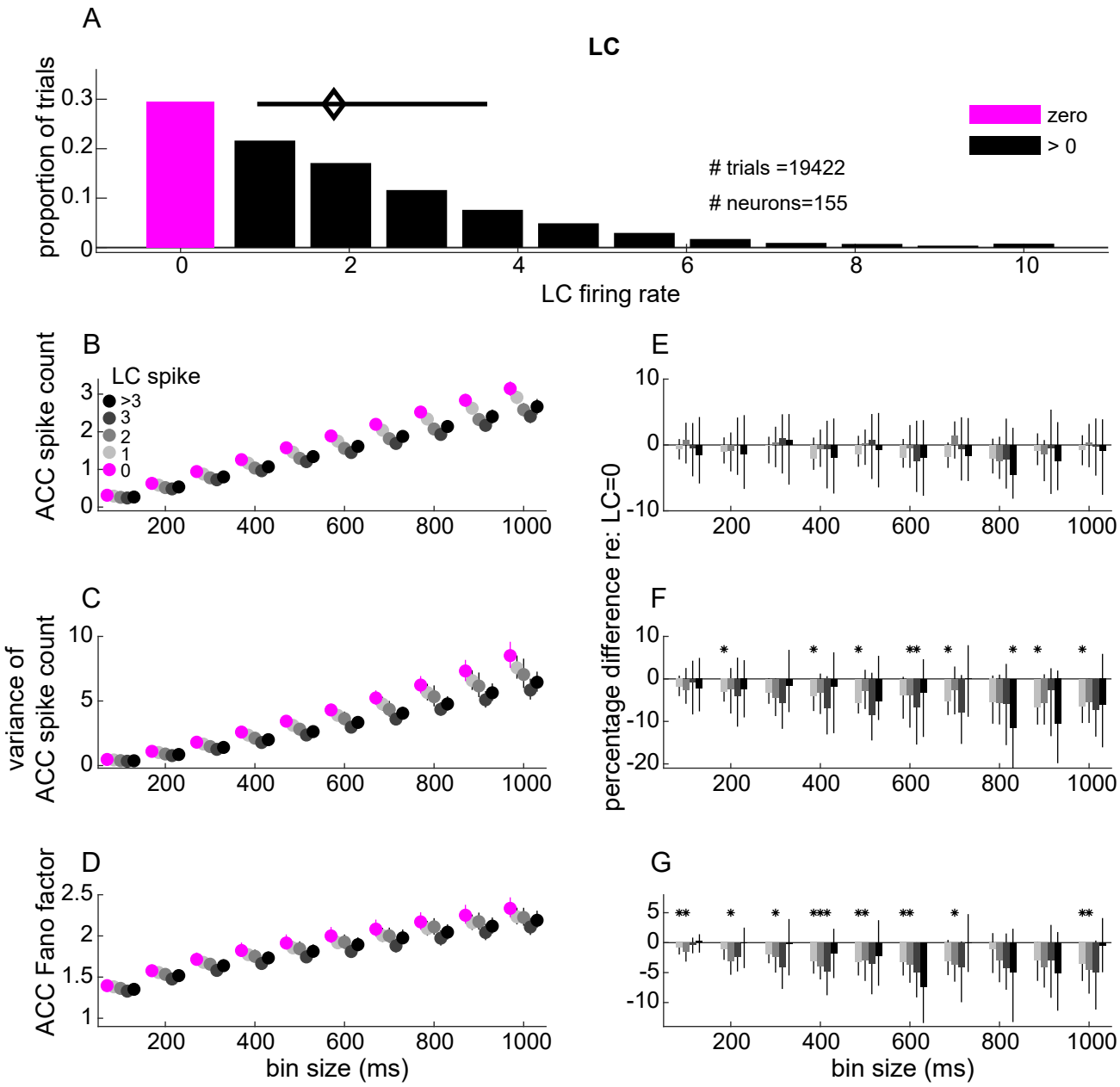

Figure 2. ACC single-unit spike count statistics conditioned on simultaneously measured LC spiking. (A) LC single-unit firing-rate distribution measured in 1.1 s windows starting 1 s after the onset of stable fixation from all trials and recording sessions. The magenta and black bars indicate the proportion of trials with zero and >0 LC spikes, respectively. The diamond and horizontal bar indicate median and IQR, respectively, from trials with ≥1 spike. (B,C,D) ACC single-unit spike count (B), variance of the spike count (C), and Fano factor (variance/mean; D) from trials in which the simultaneously measured LC unit spiked as indicated in the legend in B. ACC spikes were counted in 10 equally spaced bins ranging from 100 ms to 1 s. Symbols and error bars are mean and sem of the values computed by pooling the data across all units recorded from both monkeys. (E,F,G) Percentage difference between each value from panels A,B,C, respectively, measured in each LC>0 condition (grayscale as in the legend in panel B) versus the LC=0 condition, relative to the value from the LC=0 condition. Bars and error bars are the median and bootstrapped 95% confidence interval of the distribution of values computed per ACC unit. Symbols above indicate $p<0.05$ for sign tests for: 1) H_0: median percent difference between LCzero and LCnon-zero conditions tested separately for each monkey=0 (+; none found), and 2) H_0: median difference between LCzero and each LC spiking condition tested using data combined from both monkeys=0 (*).

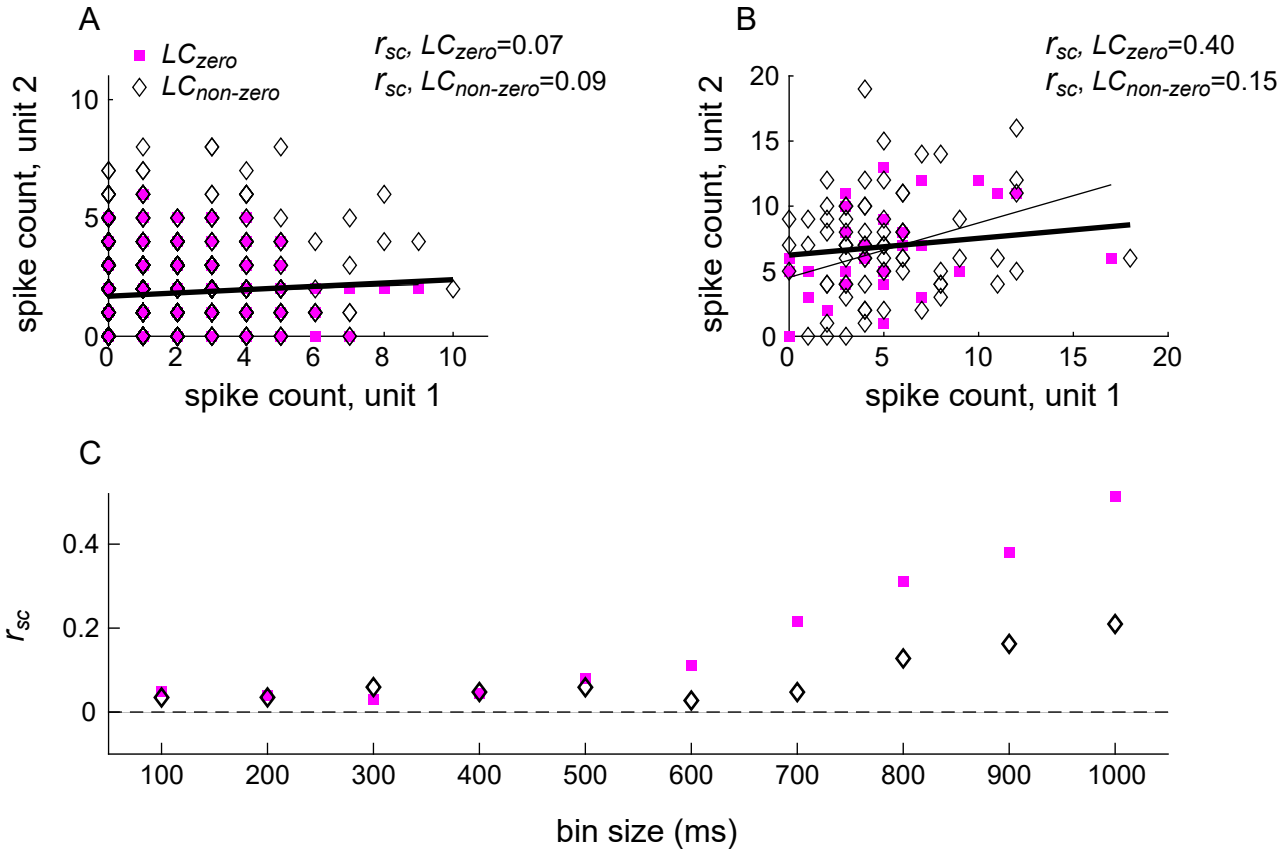

Figure 3. Spike-count correlations (r_{sc}) of an example ACC pair conditioned on the spiking activity of a simultaneously recorded LC unit. (A) ACC spikes counted in a 100 ms-wide bin. (B) ACC spikes counted in a 1000 ms-wide bin. In A and B, square/diamond markers indicate data from trials in which the simultaneously recorded LC unit had zero/non-zero firing rates. Thin/thick lines are linear fits to these data points, respectively. (C) Spike-count correlation (r_{sc}) for the example ACC pair shown in A and B as a function of bin size, computed separately for trials in which the simultaneously recorded LC unit had zero/non-zero firing rates, as indicated in A.

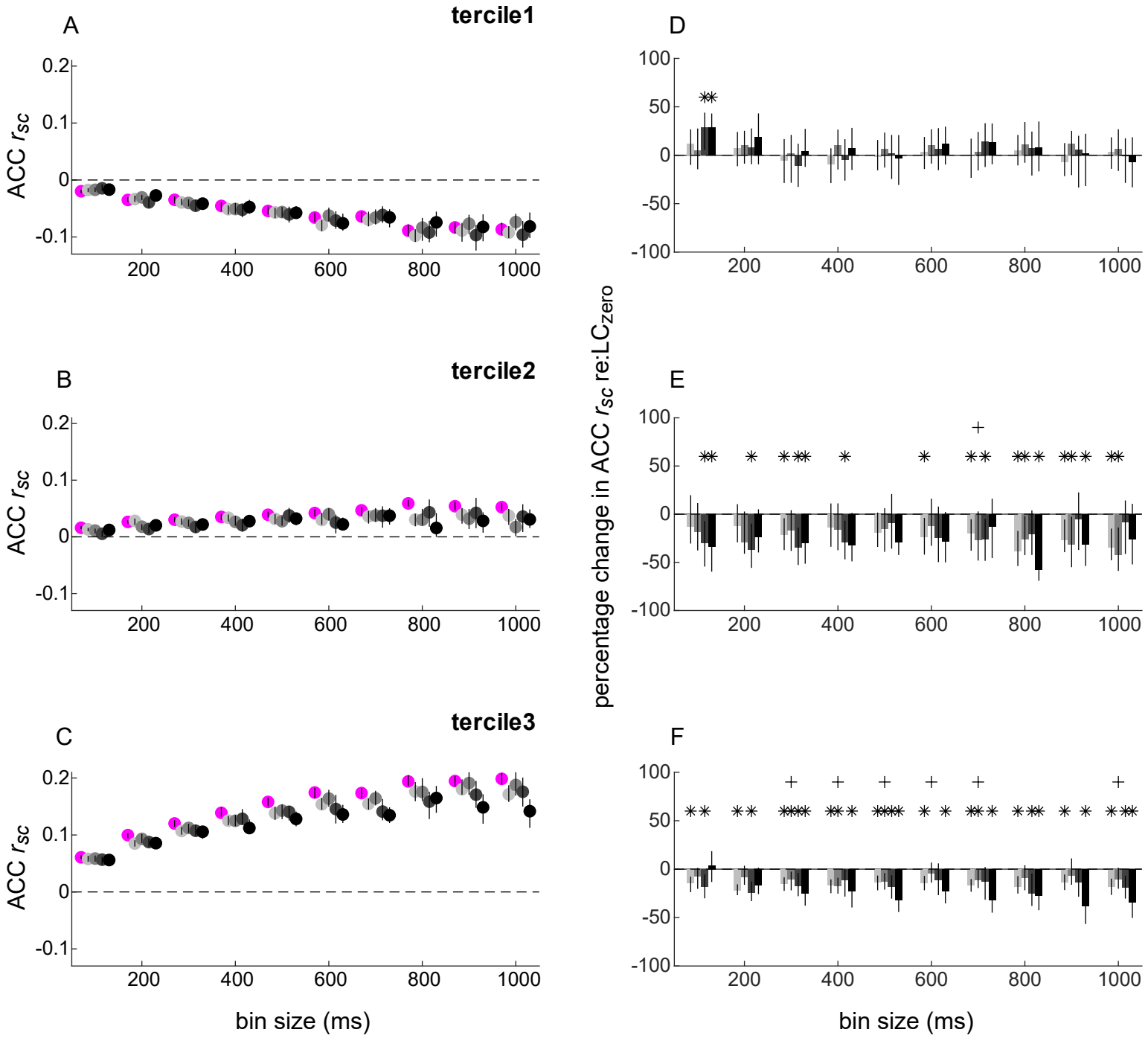

Figure 4. Spike-count correlations (r_{sc}) within ACC conditioned on simultaneously measured LC spiking. (A,B,C) ACC r_{sc} plotted as a function of bin size for each LC spike condition indicated in the legend in A. The three panels separate data by ACC pairs with r_{sc} values that, without reference to LC firing and for each bin size, were in the lower (A), middle (B), or upper (C) tercile from all recorded ACC pairs. Symbols and error bars are mean and sem across the given set of ACC pairs. (D,E,F) Percentage difference in ACC r_{sc} between each LC>0 condition and the LC=0 condition, relative to the LC=0 condition, computed for each ACC pair and plotted separately for the terciles in A,B,C, respectively. Bars and error bars are median and bootstrapped 95% confidence intervals across the given set of ACC pairs. Symbols above indicate p<0.05 for sign tests for: 1) H_0: median difference between LC$_{zero}$ and LC$_{non\text{-}zero}$ conditions tested separately for each monkey=0 (+), and 2) H_0: median difference between LC$_{zero}$ and each LC spiking condition tested using data combined from both monkeys=0 (*).

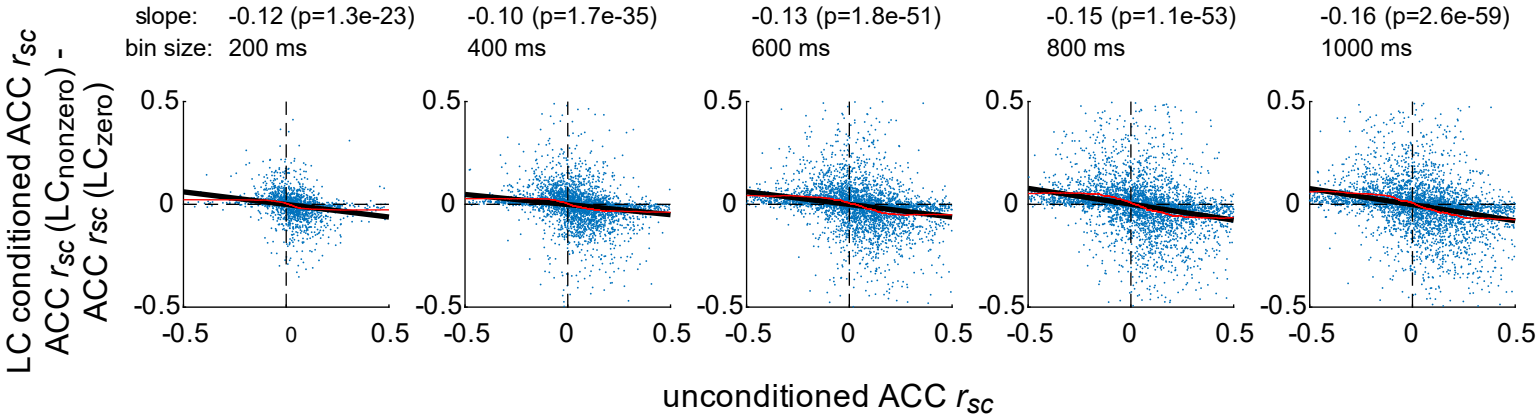

Figure 5. Relationship between the difference in ACC r_{sc} for $LC_{non\text{-}zero}$ versus LC_{zero} conditions as a function of unconditioned ACC r_{sc}. Points are data from individual ACC pairs using spikes counted in different-sized time bins, as indicated. A 500-sample running mean is shown in red, and a linear fit to the data is shown in black. Slopes and p-values for H_0: slope=0 are shown above each panel (p<0.05 for all slopes tested separately for each monkey).

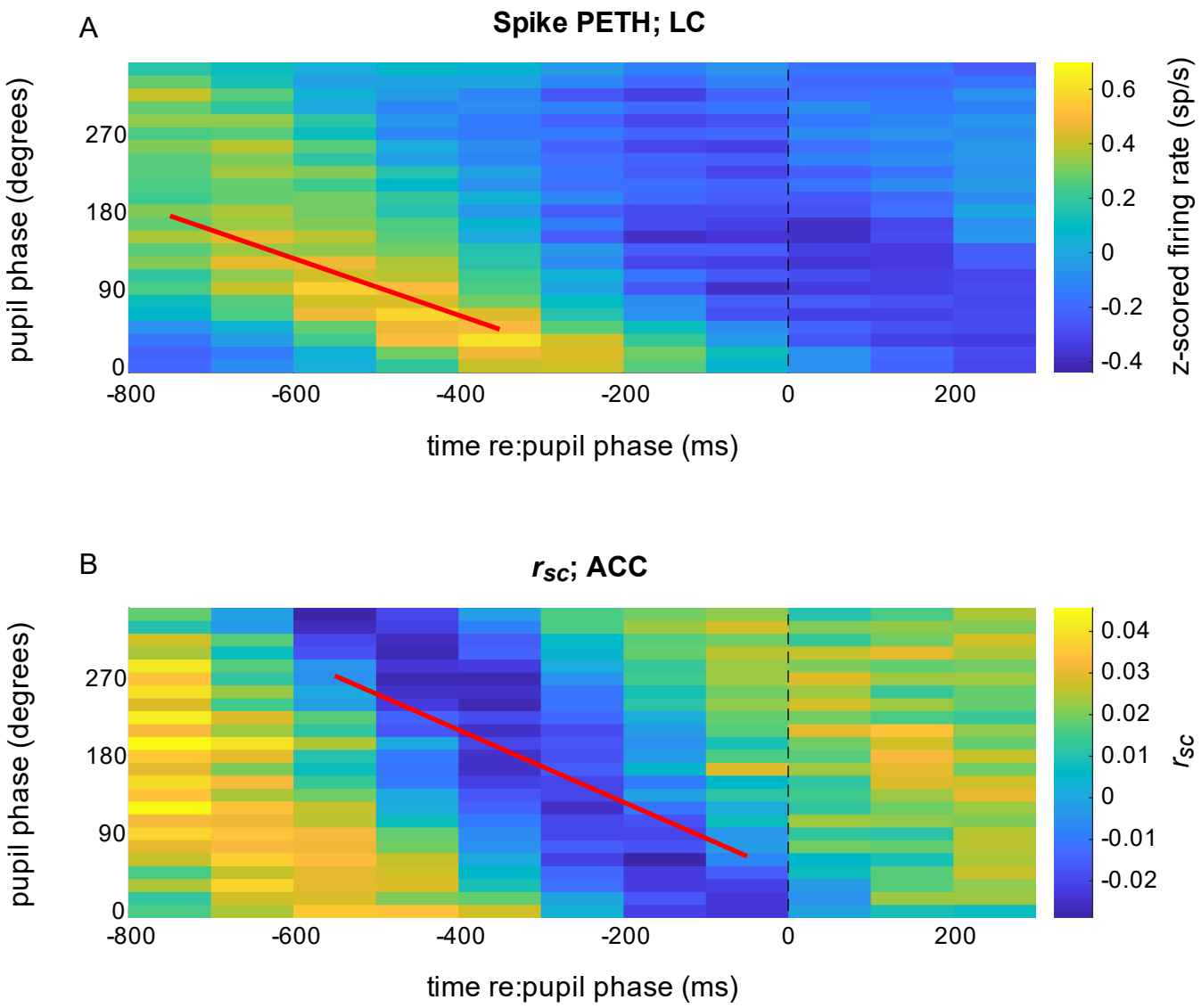

Figure 6. Spiking responses of LC neurons and correlated activity in ACC relative to pupil phase. (A) Mean LC spike rate (colormap, in sp/s z-scored per unit) computed in 500 ms-wide bins aligned to the time of occurrence of each pupil phase. For each complete pupil cycle, phase is defined with respect to the maximum rate of dilation (0°), the maximum size (90°), the maximum rate of constriction (180°), and the minimum size (270°; see Figure 6, Figure Supplement 1). Thus, the color shown at time=t (abscissa), phase=p (ordinate) corresponds to the mean spiking rate from all LC neurons that occurred in a 500 ms-wide bin centered t ms relative to the time of pupil phase p. Diagonal structure with a slope of ~-0.6 deg/ms implies a consistent relationship between LC firing and pupil phase for the given range of temporal offsets and pupil fluctuations, or hippus, that have a period of ~600 ms (Joshi et al 2016). (B) ACC r_{sc} aligned to pupil phase, computed as in A. In both panels, data are combined from all sessions for visualization. Lines are plotted using the median regression coefficients from statistically reliable linear fits (H_0: slope=0, p<0.05) to the maxima of phase-aligned LC spiking computed per unit (A; median [IQR] slope=-0.33 [-0.41 -0.30] deg/ms) and minima of the phase-aligned ACC r_{sc} computed per ACC pair (B; slope=-0.41 [-0.46 -0.35] deg/ms).

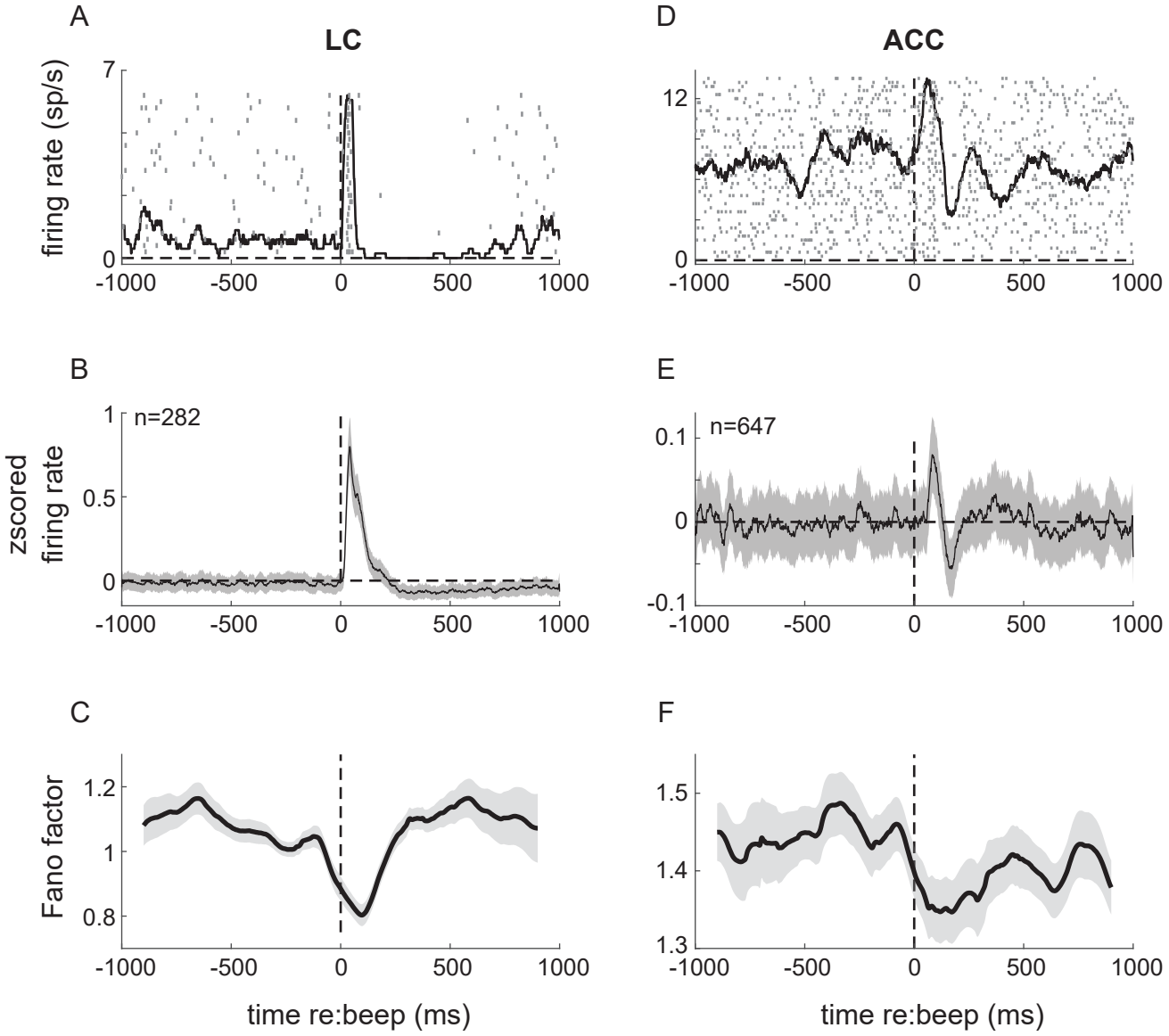

Figure 7. Neuronal responses to startling events (beep trials) in LC (left) and ACC (right). (A) Example LC unit spike raster and PSTH relative to beep onset. (B) LC population average response. (C) Fano factor as a function of time relative to beep onset, calculated in 200 ms windows. (D, E, F) ACC responses relative to beep onset plotted as in A–C. Lines and ribbons in B, C, E, and F indicate mean±sem across all trials for all monkeys.

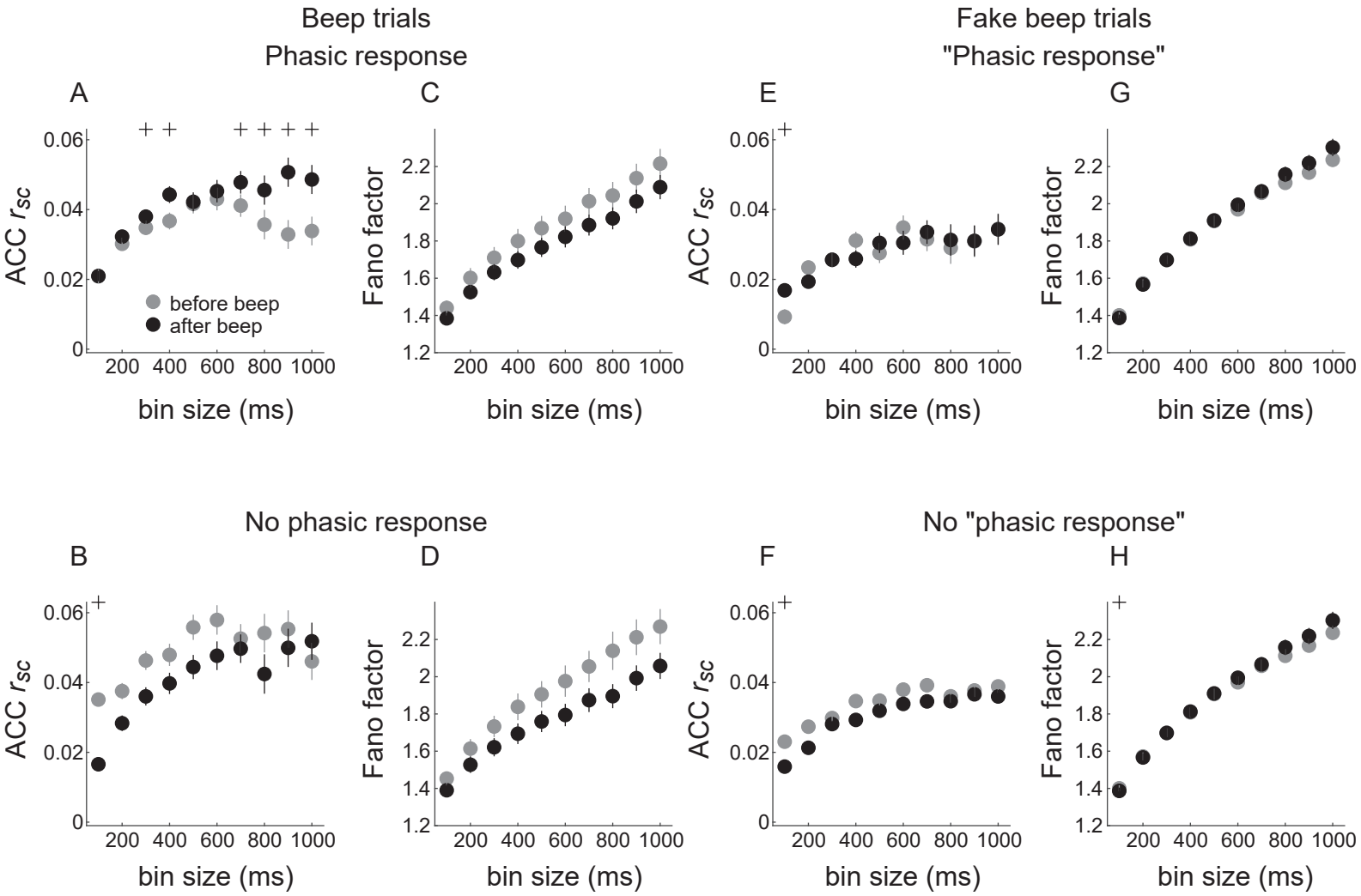

Figure 8. Changes in correlated activity in ACC in response to startling events, conditioned on LC spiking. (A) ACC r_{sc} from before (gray markers) and after the beep (black markers) for trials in which LC had a phasic response, plotted as a function of the bin size used to count spikes in ACC. Circles and vertical lines show mean±sem across sessions and monkeys. (B) Data from trials in which LC did not respond to the beep, plotted as in A. (C, D) Fano factor before (gray) and after (black) the beep for ACC single neurons, plotted as in A and B. (E–G) Data from “fake-beep trials” (trials with no beep but sorted according to whether or not there was a transient increase in LC spiking comparable in magnitude to the beep-evoked response), plotted as in A–D. In all panels, + indicates sign-rank test for H_0: median difference in r_{sc} before versus after the beep for the given time bin, $p<0.05$ for each monkey tested separately.

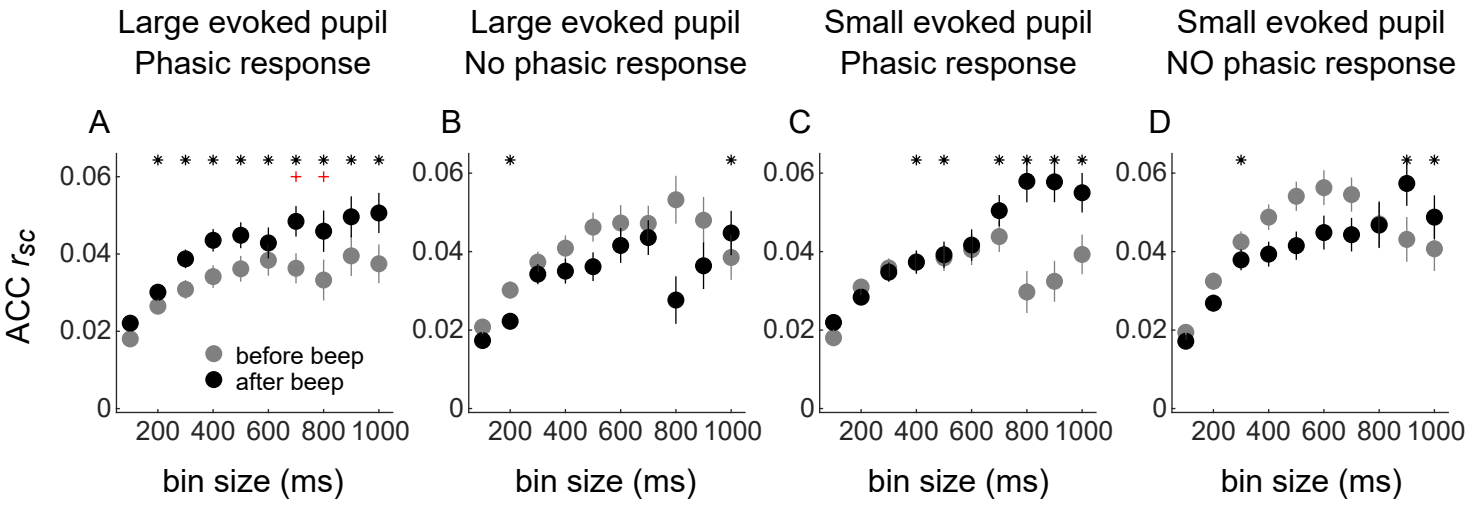

Figure 9. Startle-linked changes in ACC correlations relative to LC and pupil responses. (A) ACC r_{sc} plotted as a function of bin size for trials in which a phasic LC response was accompanied by a large pupil dilation. (B) ACC r_{sc} for trials in which there was a large evoked pupil dilation but no phasic LC response. (C) ACC r_{sc} for trials in which a phasic LC response was accompanied by a relatively smaller evoked pupil dilation. (D) ACC r_{sc} for trials in which there was a small evoked pupil dilation and no phasic LC response. All symbols and error bars are mean±sem across ACC pairs from both monkeys. * symbols at the top of each panel indicate sign-rank test for H_0: median difference in r_{sc} before versus after the beep for the given time bin, $p<0.05$ for each monkey tested separately. Red symbols at the top of A indicate bin-specific effects (ANOVA, $p<0.05$) of pupil size (large versus small; none significant), LC phasic response (yes versus no; +), and their interaction (none significant).

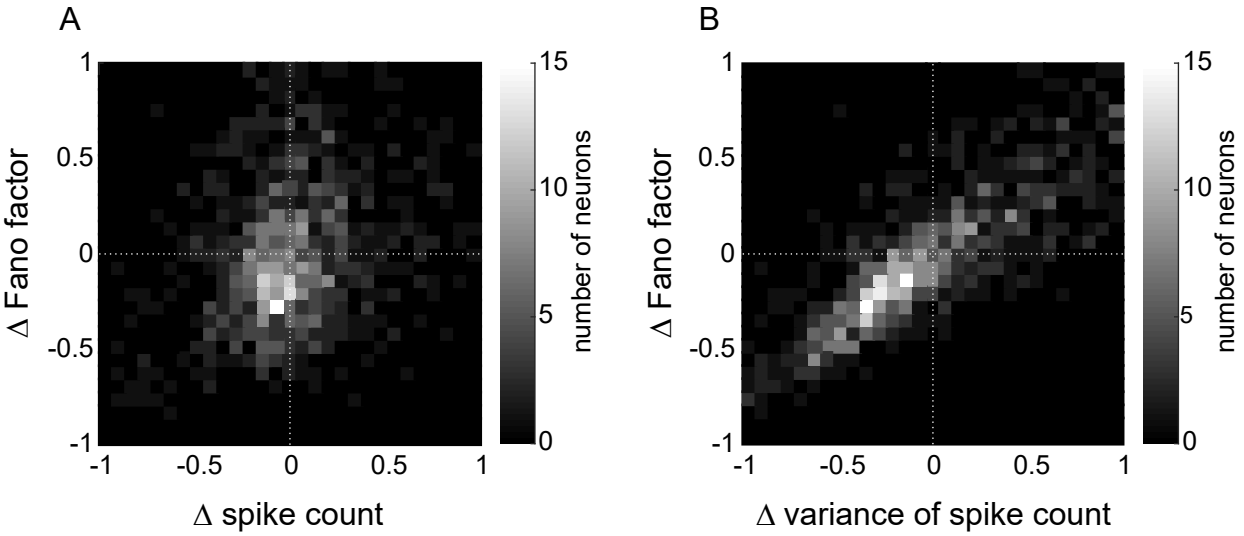

Figure 2 – Figure Supplement 1. ACC single neuron spike count and variability conditioned on LC spiking (measured as differences between measurements from $LC_{non\text{-}zero}$ versus LC_{zero} trials). (A). Relationship between difference in Fano factor and difference in spike count. (B) Relationship between difference in Fano factor and difference in variance of spike count.

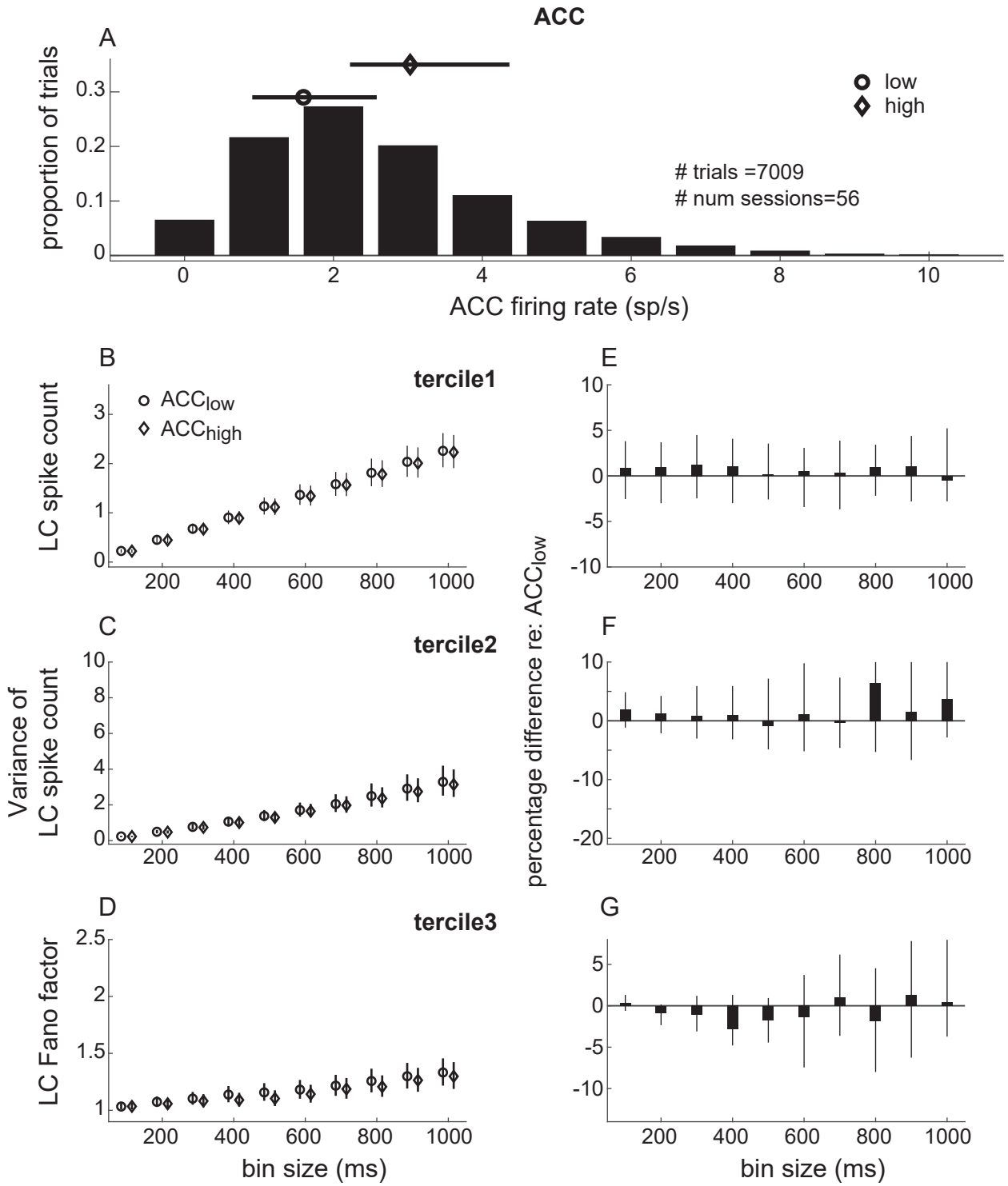

Figure 2 – Figure Supplement 2. LC single-unit spike count statistics conditioned on simultaneously measured ACC spiking. (A) ACC single-unit firing-rate distribution measured in 1.1 s windows starting 1 s after the onset of stable fixation from all trials and recording sessions. The circle and diamond symbols and lines indicate the median and IQR of trials defined as “low” and “high” ACC spike counts (median split per session), respectively. (B–D) LC single-unit (B) spike count, (C) variance of spike count, and (D) Fano factor (variance/mean) from trials in which the simultaneously measured ACC unit had low or high spiking activity as indicated by the markers defined in B. LC spikes were counted in 10 equally spaced bins ranging from 100 ms to 1 s. Symbols and error bars are mean ± sem of the values computed by pooling the data across all units recorded from both monkeys. (E,F,G) Percentage difference between each value from panels B,C,D, respectively, measured in the ACC low- versus high-spiking condition, relative to the low-spiking condition. In all cases, signtest for H_0: median percent change=0, p>0.05 for both monkeys tested separately or together.

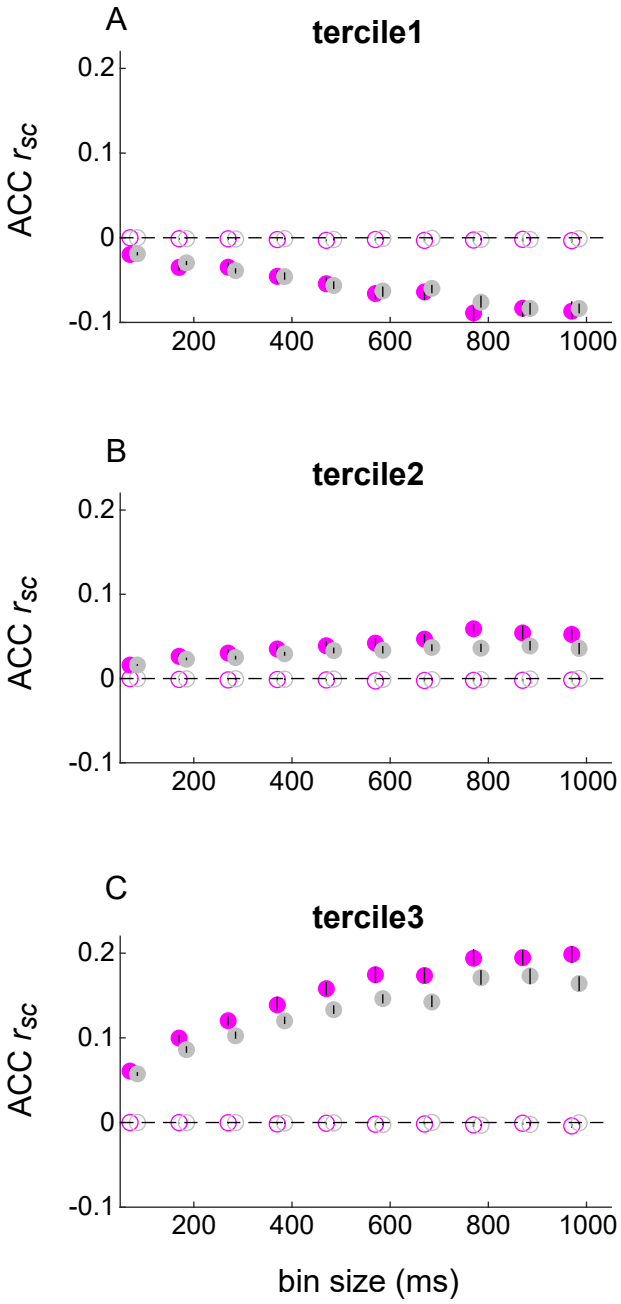

Figure 4 – Figure Supplement 1. Confidence estimates of ACC r_{sc} conditioned on simultaneously measured LC spiking using shuffled trials. Solid markers show unshuffled ACC *rsc* data conditioned on LC spiking, separated into terciles (panels) of LC-independent values, plotted as in Figure 4A–C for LC_{zero} and $LC_{non\text{-}zero}$ trials. Open markers show ACC *rsc* from shuffled data. Bootstrapped 95% confidence intervals are plotted as vertical bars (too small for visibility in most cases).

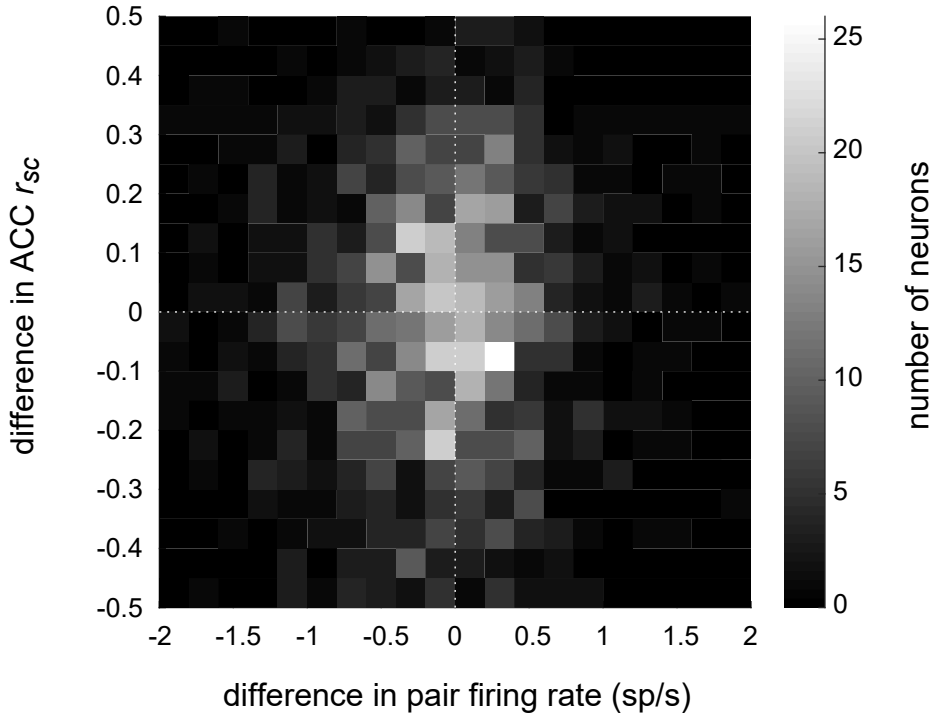

Figure 4 – Figure Supplement 2. Relationship between LC-linked differences in ACC r_{sc} and ACC mean firing rate. For each simultaneously recorded pair of ACC units and single LC unit, the difference in ACC r_{sc} computed from $LC_{non\text{-}zero}$ versus LC_{zero} trials (ordinate) is plotted versus the difference in the mean spike rate of the two ACC units computed from $LC_{non\text{-}zero}$ versus LC_{zero} trials (abscissa). Spearman's *rho*=0.007, p=0.8.

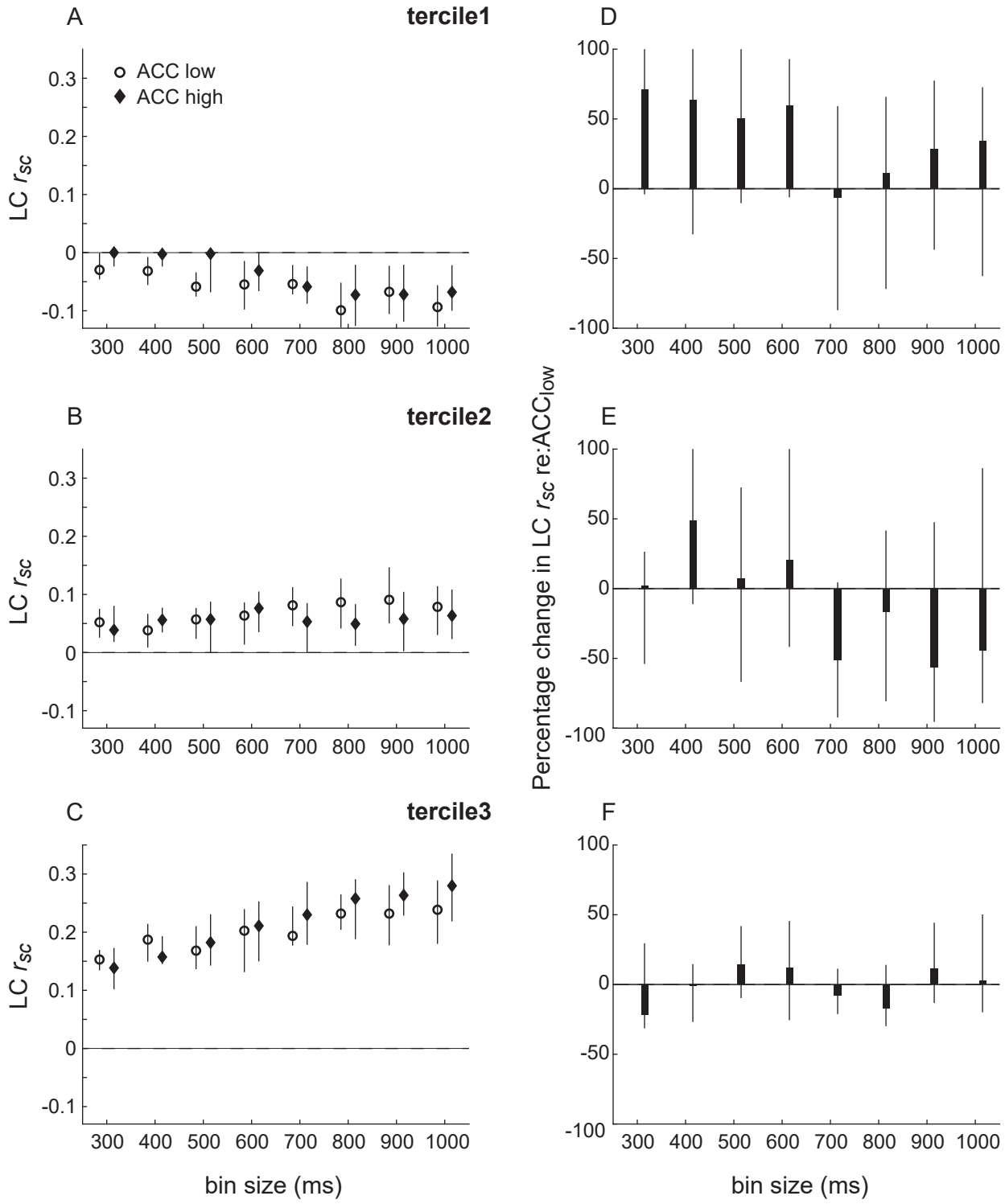

Figure 4 – Figure Supplement 3. Spike-count correlations (*rsc*) within LC conditioned on simultaneously measured ACC spiking. (A,B,C) LC *rsc* plotted as a function of bin size separately for trials in which the simultaneously recorded ACC unit had a relatively low or high firing rate, as indicated in A. The three panels separate data by LC pairs with *rsc* values that, without reference to ACC firing and for each bin size, were in the lower (A), middle (B), or upper (C) tercile from all recorded LC pairs. Symbols and error bars are mean and sem across the given set of LC pairs. (D,E,F) Percentage difference in LC *rsc* between ACC low versus ACC high conditions, relative to the ACC low condition, computed for each LC pair and plotted separately for the terciles in A,B,C, respectively. Bars and error bars are median and bootstrapped 95% confidence intervals across the given set of LC pairs. In all cases, sign test for *H0*: median percent change=0, *p*>0.05 for both monkeys tested separately or together.

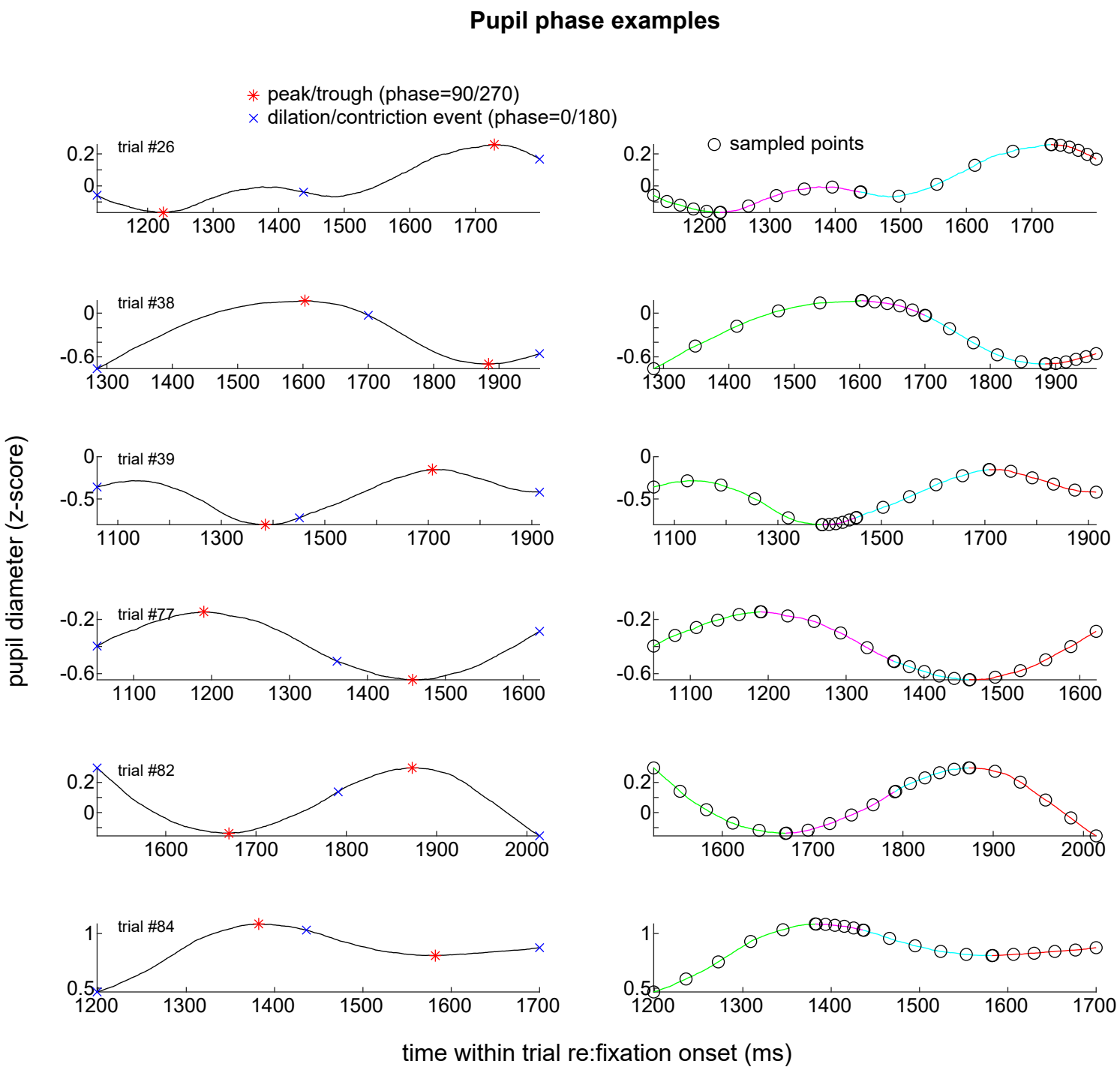

Figure 6 – Figure Supplement 1. Pupil phase examples. Example pupil traces from individual trials (rows) showing principal phases (left; 0°, 90°, 180°, and 270°) and intermediate sampled points (right) used in pupil analyses.

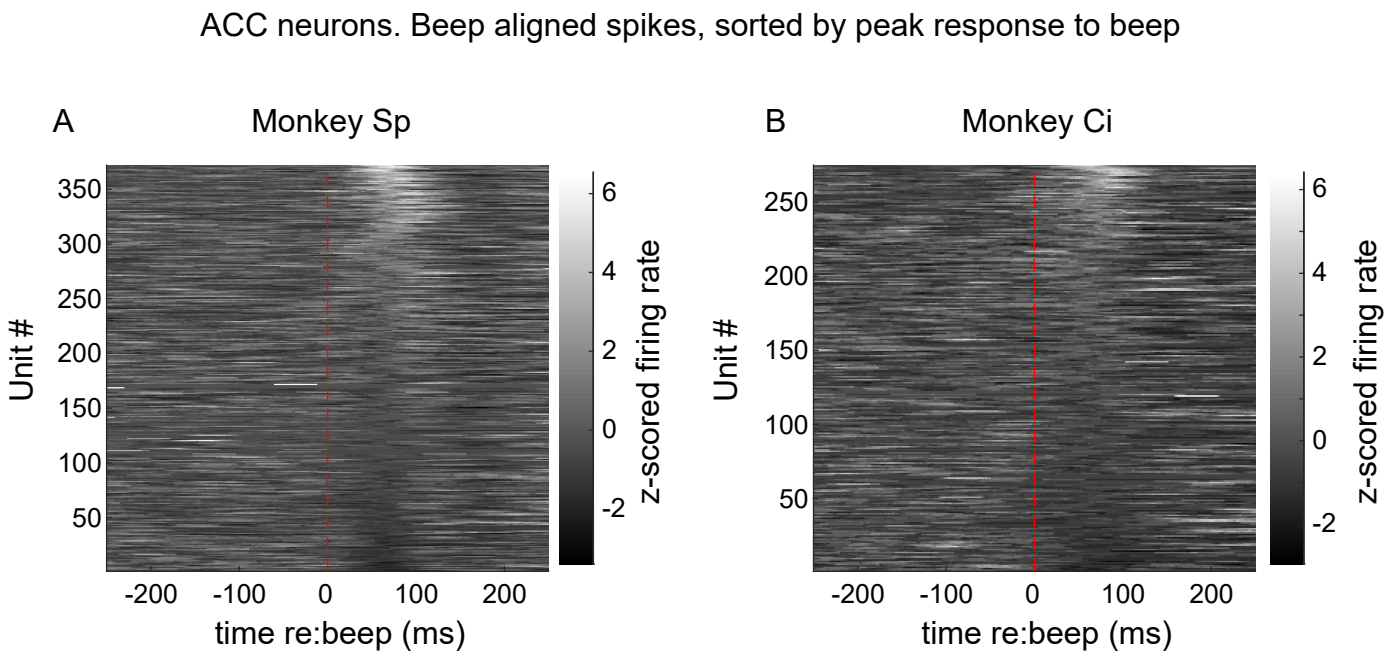

Figure 7 – Figure Supplement 1. ACC single-unit responses to the startle stimulus (beep). Average PSTHs aligned to beep onset from all units recorded from Monkey Sp (A) and monkey Ci (B).

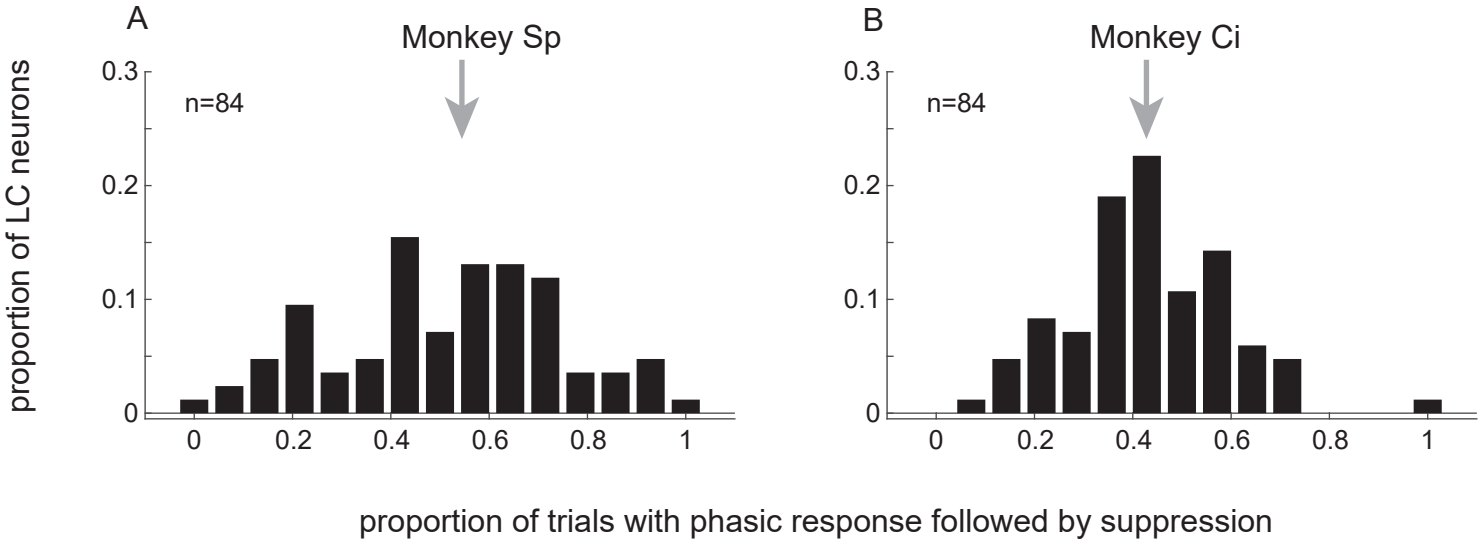

Figure 8 – Figure Supplement 1. Consistency of LC responses to startling sounds. Histograms showing the proportion of LC neurons from monkey Sp (A) and Ci (B) that exhibited a characteristic phasic response followed by post-phasic suppression for the given proportion of beep trials. Arrows indicate median values.

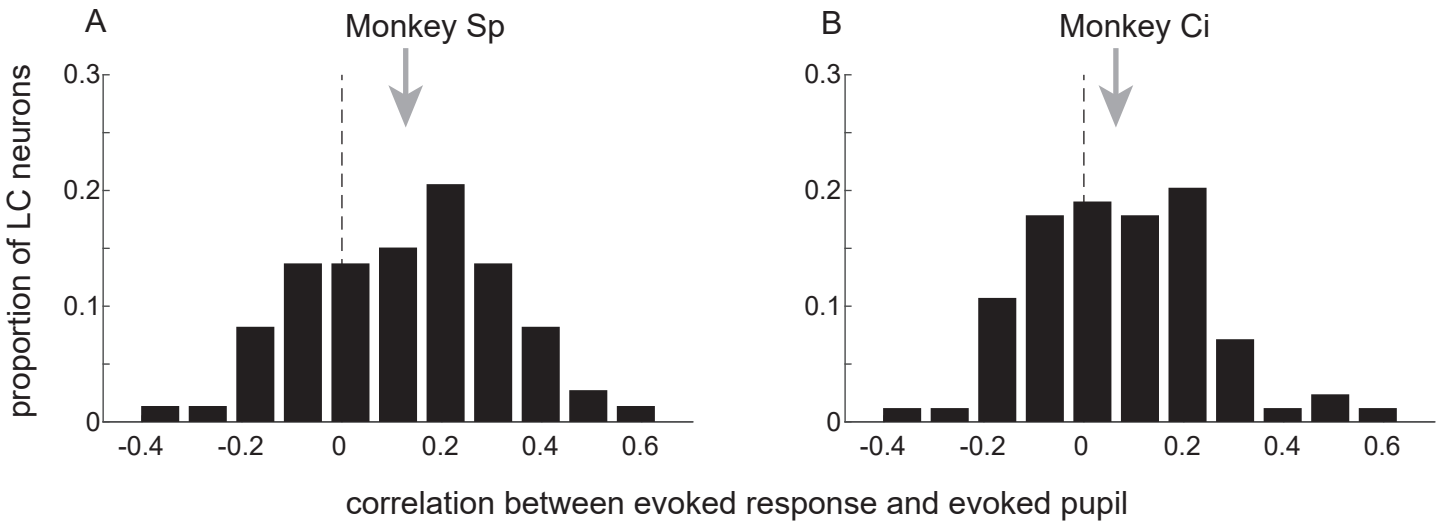

Figure 9 – Figure Supplement 1. Relationship between startling sound-driven changes in pupil diameter and LC phasic activation. Distribution of correlation coefficients describing unit-specific relationships between the size of the pupil response and the size of the LC phasic response to beep presentation for monkey Sp (A) and Ci (B). Arrows indicate median values (sign-rank test for H_0: median=0, p<0.001 in both cases).